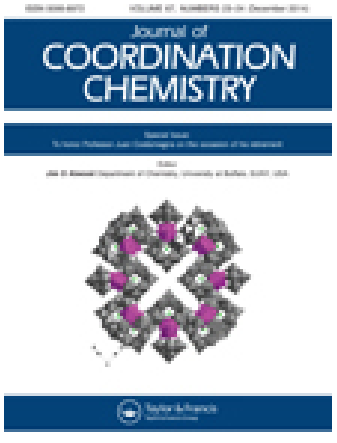

Journal of Coordination Chemistry
Publication details, including instructions for authors and subscription information:
http://www.tandfonline.com/loi/gcoo20

Coordination and organometallic compounds in the functionalization of carbon nanotubes

Boris I. Kharisov[ac] & Oxana V. Kharissova[bc]

[a] Department of Chemistry, Universidad Autónoma de Nuevo León, Monterrey, Mexico

[b] Department of Physico-Mathematics, Universidad Autónoma de Nuevo León, Monterrey, Mexico

[c] CIIDIT, Universidad Autónoma de Nuevo León, Monterrey, Mexico

Accepted author version posted online: 30 Jan 2014.Published online: 04 Mar 2014.

Journal of Coordination Chemistry, 2014
Vol. 67, Nos. 23–24, 3769–3808, http://dx.doi.org/10.1080/00958972.2014.888063

REVIEW

Coordination and organometallic compounds in the functionalization of carbon nanotubes

BORIS I. KHARISOV*†§ and OXANA V. KHARISSOVA‡§

†Department of Chemistry, Universidad Autónoma de Nuevo León, Monterrey, Mexico
‡Department of Physico-Mathematics, Universidad Autónoma de Nuevo León, Monterrey, Mexico
§CIIDIT, Universidad Autónoma de Nuevo León, Monterrey, Mexico

(*Received 13 August 2013; accepted 4 October 2013*)

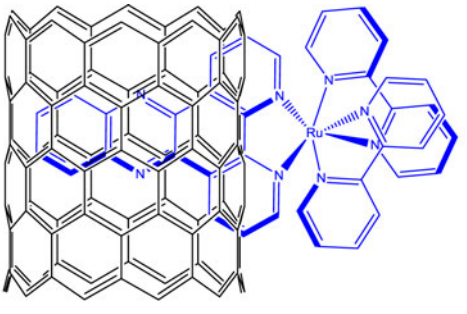

Various methods for functionalization of carbon nanotubes (CNTs) using classic coordination complexes, as well as organometallic compounds as precursors, are discussed. CNTs can form hybrids via covalent or non-covalent interaction with metal complexes of crown ethers, carboxylates, amines, polypyridyl compounds, a host of N,O-containing ligands, derivatives of phosphonic acid, porphyrins, phthalocyanines, carbonyls, cyclopentadienyls, pyrene-containing moieties, and other aromatic structures. Several applications of synthesized composites/hybrids are emphasized.

Keywords: Metal complexes; Carbon nanotubes; Graphene; Functionalization; Cyclopentadienyls; Ruthenium complexes

Introduction

Metal complexes have applications in organic and organometallic chemistry, catalysis [1], in medicine as anticancer pharmaceutics and for drug delivery [2], in various biological systems [3], polymers [4] and dyes, separation of isotopes [5] and heavy metals [6], etc. Sometimes, they are applied for increasing solubility [7, 8] of classic objects; carbon nanotubes (CNTs),

*Corresponding author. Email: bkhariss@hotmail.com

which form bundle-like structures with very complex morphologies with a high number of van der Waals interactions, have extremely poor solubility in water or organic solvents. Metal complexes also serve as precursors to fill CNTs with metals [9] or oxides [10], to decorate CNTs with metal nanoparticles [11], as well as to be encapsulated by CNTs [12].

Various techniques are applied to obtain functionalized CNTs [13–15]. Figure 1 shows functionalization possibilities for single-walled CNTs (SWNTs), some of which will be discussed below for several metal complexes. The simplest functionalization by mineral acids, usually used as a first step, leads to formation of –OH and –COOH groups, which further can be replaced with more complex organic moieties. In particular, as shown below, a series of coordination and organometallic compounds have been anchored onto CNTs by covalent or non-covalent mode. In this review, we describe peculiarities of functionalization of CNTs with metal complexes, paying particular attention to the ligand type (N-, O-, N,O-, N,S-, N,P-containing moieties), bond type inside complexes {coordination bond M–O, M–N, M–S, M–P; σ- and π-metal-carbon bond in organometallics}, and interaction type between CNTs and complex. Representative examples for the synthesis of CNTs hybrids/composites with metal complexes are shown in table 1 and their main applications in table 2.

Composites of CNTs with metal complexes of O-containing ligands

A few crown ethers have been used for CNTs functionalization, showing higher dispersibility of formed hybrids. Thus, SWNTs may be made soluble in a range of organic

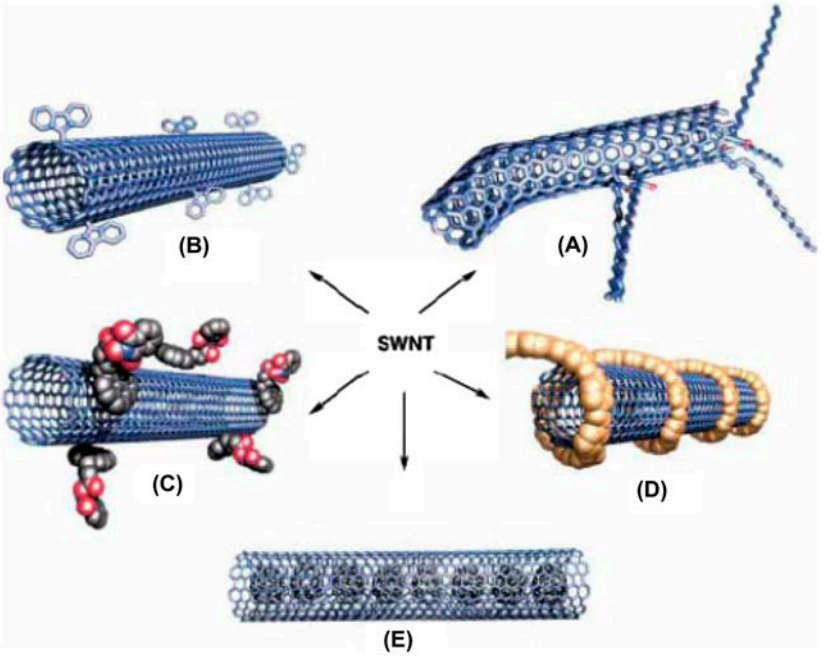

Figure 1. Functionalization possibilities for SWNTs: (A) defect-group functionalization, (B) covalent sidewall functionalization, (C) non-covalent functionalization with surfactants, (D) non-covalent exohedral functionalization with polymers, (E) endohedral functionalization [16].

Table 1. Overview of representative examples on the synthesis of metal-complex-FCNTs.

Composite of metal complex with CNTs	Conditions/procedure	References
Complexes of organic acids or crown-ethers		
$[Na(dibenzo\text{-}18\text{-}crown\text{-}6)]_n[SWNT]$	Reduction of CNTs by Na/Hg amalgam in the presence of dibenzo-18-crown-6	[17]
$\{MWCNTs@Cu_3(btc)_2\}$ (btc = 1,3,5-benzenetricarboxylate)	Solvothermal synthesis	[20]
Complexes of amines, polypyridil ligands, Schiff bases, porphyrins, and phthalocyanines		
Cobalt chloride complexed aminoalkylalkoxysilane FCNTs (fluorinated CNTs)	Reaction of *N*-[3-(trimethoxysilyl)propyl] ethylenediamine with FCNTs produced the corresponding aminoalkylalkoxysilane FCNTs. Cobalt salt was then complexed to these FCNTs by the addition of cobalt chloride to form cobalt complexed nanocomposite	[22]
Ruthenium *tris*(bipyridyl) complex linked through peptidic bonds to SWCNTs	Radical addition of thiol-terminated SWCNT to a terminal C=C double bond of a bipyridyl ligand of the ruthenium *tris*(bipyridyl) complex	[27]
SWCNT–Cu^{2+} complex with stearic acid (SA) or ethylenediaminetetraacetic acid (EDTA)	A metal coordination reaction in ultrasonic conditions (before ligand coordination)	[34]
SWCNTs modified with metal-free porphyrin units	Electropolymerization of pyrrole or pyrrole-substituted porphyrin monomers or interaction between glycyl-substituted porphyrin and non-modified CNTs	[42]
SWCNT-PVP·Zn(TPP) nanohybrid {PVP = poly(4-vinylpyridine); (TPP = tetraphenyl porphyrin)}	Dispersible SWCNTs grafted with poly(4-vinylpyridine), SWNT-PVP, were tested in coordination assays with zinc tetraphenylporphyrin {Zn(TPP)}	[43]
CNTs/MPc nanohybrids	A mixture of FePc, CoPc, FePh or CoPh, and MWCNTs in isopropanol was prepared and sonicated for 30 min followed by magnetic stirring for 1 h	[52]
Complexes of sulfur-containing ligands		
$[PPh_4][Cu(DMED)_2]$ (DMED = 1,2-dicarbomethoxy-1,2-dithiolate)	The reaction between a copper polysulfide precursor and activated acetylene, formation of nanospheres and their further aggregation with water soluble (carboxylated) carbon nanotubes (wsCNTs)	[60]
Cyclopentadienyls, carbonyls, and π-complexes with aromatic compounds		
Cp_2ZrCl_2/MWCNTs	Direct adsorption of Cp_2ZrCl_2 onto MWCNTs	[61]
Ferrocene derivatives, π-stacked or covalently grafted onto a film of CNTs	The immobilization of the ferrocene moiety via π–π interactions was done with a ferrocene derivative bearing a pyrene group. The covalent grafting on the film of CNTs was achieved in two steps via the electroreduction of an aminoethyl-benzenediazonium salt followed by post-functionalization with an activated ester derivative of ferrocene	[69]
$(\eta^6\text{-SWNT})Cr(CO)_3$, $(\eta^6\text{-SWNT})Cr(\eta^6\text{-}C_6H_6)$, $(\eta^6\text{-SWNT})_2Cr$	Reactions of SWNT and SWNT-CONH $(CH_2)_{17}CH_3$ with chromium hexacarbonyl and $(\eta^6$-benzene)chromium tricarbonyl	[72]
A multifunctional block copolymer incorporated with pyrene and ruthenium terpyridyl thiocyanato complex moieties	Reversible addition–fragmentation chain transfer polymerization	[76]
Cobalt *bis*(4-pyren-1-yl-*N*-[5-([2,2′;6′,2″] terpyridin-4′-yloxy)-pentyl]-butyramide) functionalized SWNTs	Direct functionalization SWNTs via non-covalent π–π stacking interactions	[77]

solvents without sidewall functionalization via their reduction by Na/Hg amalgam in the presence of dibenzo-18-crown-6 [17]. The $[Na(dibenzo\text{-}18\text{-}crown\text{-}6)]_n[SWNT]$ complex was consistent with no additional sidewall functionalization as compared with raw

Table 2. Overview of representative examples on the applications of metal-complex-FCNTs.

Composite of metal complex with CNTs	Applications	References
Organic acids, crown-ethers		
{MWCNTs@Cu_3(btc)$_2$} (btc = 1,3,5-benzenetricarboxylate)	Determination of trace levels of lead	[20]
Li@CNT@[Cu_3(btc)$_2$]	Uptakes of CO_2 and CH_4	[21]
Complexes of amines, polypyridil ligands, Schiff bases, porphyrins, and phthalocyanines		
Ethylenediamine-functionalized CNTs	Good capacity to retain Hg^{2+} from complex matrix including fish and real water samples	[23]
Tris(2,2′-bipyridyl)ruthenium(II) {Ru(bpy)$_3^{2+}$}/CNTs	Electrogenerated chemiluminescence (ECL) sensor for TPA	[24]
Nickel *salen* and *salophen* complexes/CNTs	Catalysis for oxidation of primary and secondary alcohols	[28–31]
MWCNTs-palladium(II)-Schiff base complex	Efficient catalysis in the coupling reactions of acid chlorides with terminal alkynes under copper-, phosphorous-, and solvent-free conditions in air	[33]
Fe^{III}-DETPA complex/CNTs	Sensor to hydrogen peroxide	[35]
Hybrid Ag-containing CNTs-composites on the basis of ligands *N*-(2-vinylsulfanyl-ethylidene)-benzene-1,2-dimine, *N*-pyridin-2-ylmethylene-benzene-1,2-dimine, and *N*-furan-2-ylmethylene-benzene-1,2-dimine	Ionophores and as ion–electron transducers to construct Ag^+ carbon paste electrodes	[38]
Mixed assembly of ferrocene/porphyrin onto carbon nanotube arrays	Candidates for molecular memory devices	[46]
SWCNT doped with porphyrin-like nitrogen defects (4ND-CNxNT) with 10 different transition metals (TMs = Sc, Ti, V, Cr, Mn, Fe, Co, Ni, Cu, and Zn)	Hydrogen storage	[48]
Phthalocyanine and porphyrin-functionalized MWCNTs	Non-precious electrocatalysts for the electroreduction of oxygen	[51]
FePc coated on SWCNTs	Methanol oxidation in the ORR (organic reduction reaction)	[55]
Hybrid material composed of SWNTs and CoPc derivatives	Excellent sensitivity and selectivity to dimethyl methylphosphonate (DMMP) (stimulant of nerve agent sarin)	[56]
Cyclopentadienyls, carbonyls, and π-complexes with aromatic compounds		
SWNTs and MWNTs covalently functionalized with a titanium alkoxide catalyst containing cyclopentadienyl (Cp)	Surface initiated titanium-mediated coordination polymerizations of L-lactide, ε-caprolactone, and *n*-hexyl isocyanate	[62]
Ferrocene-functionalized SWCNTs	Electrode for L-glutamate detection	[66]
MWCNTs functionalized with pyrene nickel complexes through π–π stacking	Robust, noble-metal-free electrocatalytic nanomaterials for H_2 evolution and uptake	[78]
CNTs nanohybrid materials containing iridium *N*-heterocyclic carbene (NHC)-type organometallic complexes	Use in heterogeneous iridium-catalyzed hydrogen-transfer reduction of cyclohexanone to cyclohexanol with 2-propanol/KOH as hydrogen source	[82]

SWNTs; the presence of the [Na(dibenzo-18-crown-6)]$^+$ ion was shown. Solubility was found to be greatest in CH_2Cl_2 and DMF being comparable to surfactant-dispersed SWNTs; measurable solubilities were also detected in hexane, toluene, and alcohols. Benzo-18-crown-6 covalently linked to multi-walled carbon nanotubes (MWCNTs) can be used as ion sensors, in particular for Pb^{2+} determination [18].

Other ligands, containing oxygen donors only, are rare. Thus, functionalization of oxidized SWCNTs by a zwitterionic interaction ($COO^-NH_3^+$) between protonated amine on crown ether and an oxyanion from a carboxylic acid group on a SWCNT was described [19]. The functionalization was achieved by adding 4-aminobenzo-9-crown-3 **1** to SWCNTs (reactions *1*). The ionic interaction led to a considerable

increase in the solubility of SWCNTs in both organic and aqueous solvents such as ethanol, DMSO, DMF, and H_2O, showing the highest solubility in DMF and DMSO. The ionic bonded 4-benzo-9-crown-3 ether allowed the hosting of Li^+ and the ionic bond of crown ether to SWCNT was identified. Important major differences of ionic functionalization to covalent functionalization are: (a) The acid–base reaction represents the simplest possible route to soluble SWNTs and can be readily scaled-up at low cost. (b) Unlike the covalent amide bond, the presence of zwitterions (ionic functionalization) can significantly improve the solubility of SWCNT-CE (crown ether) in aqueous solvents. (c) The cation in crown ether of the ionic bond of SWNT-$COO^-NH_3^+$ of SWNTs can be readily exchanged by other organic and inorganic cations. (d) The authors found that the covalent functionalization approach generally gave a higher yield (30.4%) of SWCNT-CE than the ionic functionalization approach (26%).

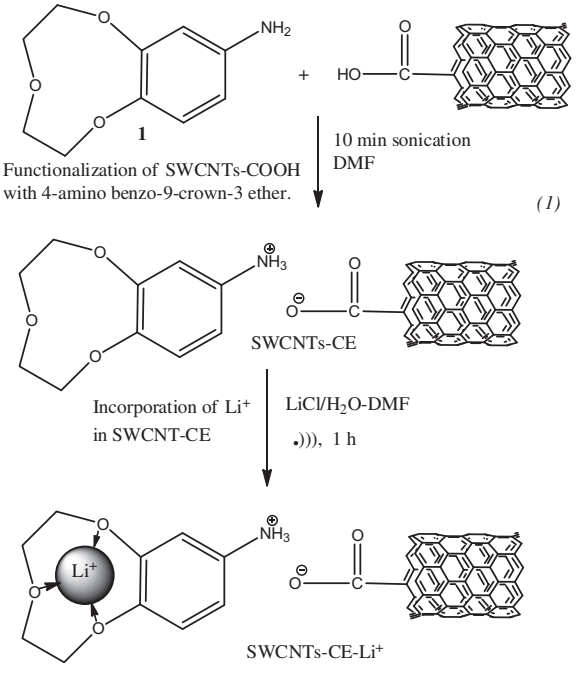

The solvothermally prepared MWCNTs-metalorganic frameworks {MWCNTs@$Cu_3(btc)_2$} (btc = 1,3,5-benzenetricarboxylate **2**) were studied for determination of trace levels of lead [20]. The experimental procedure was carried out by accumulating lead on the electrode surface and subsequently measuring with differential pulse anodic stripping voltammetry in a lab-on-valve format. The main parameters affecting the analytical performance, including the amount of MWCNTs@$Cu_3(btc)_2$ suspension, supporting electrolyte and its pH, stripping mode, and flow rate, have been investigated. Under optimum conditions, the oxidation peak current displayed a calibration response for lead over a concentration range from 1.0×10^{-9} to 5.0×10^{-8} M L^{-1} with an excellent detection limit of 7.9×10^{-10} M L^{-1}. In related research [21], Li@CNT@[$Cu_3(btc)_2$] composite was applied for uptake of CO_2 and CH_4.

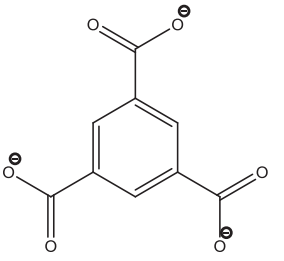

BTC anion

2

Composites of CNTs with metal complexes of N-, N,O-, and N,S-containing ligands

In an application of ligands (generally amines), containing only nitrogen donors,[†] participating in coordination with metal, we note that the reaction of *N*-[3-(trimethoxysilyl) propyl]ethylenediamine with fluorinated carbon nanotubes (FCNTs) produced the corresponding aminoalkylalkoxysilane FCNTs [22]. Cobalt salt was then complexed (reactions *2*) to these FCNTs by addition of cobalt chloride to form cobalt complexed nanocomposite in high yield. The amino-functionalization of MWCNTs with ethylenediamine (figure 2) led [23] to functionalized MWCNTs having good capacity to retain Hg^{2+} from complex matrix including fish and real water samples, in a difference with the raw and purified MWCNTs, which did not adsorb Hg^{2+}. Effective parameters on Hg^{2+} retention such as pH, flow rate, nature of the eluent, the ionic strength, selectivity coefficient, and retention capacity were studied, revealing, in particular, that the enrichment factor and maximum capacity of the sorbent were 100 mL and 11.58 mg/g, respectively. Selectivity experiments showed that the adsorbents have a stronger specific retention for Hg^{2+} than Fe^{3+}, Cu^{2+}, Pb^{2+}, Ni^{2+}, Mn^{2+}, Ca^{2+}, and Mg^{2+}. The Hg^{2+} ions adsorbed by amino-functionalized MWCNTs were mainly aggregated on the ends and at the defect sites on the amino-functionalized MWCNTs. The sorption mechanism appears mainly attributable to supramolecular interaction between the mercury ions and the surface functional groups of amino-functionalized MWCNTs which have a negative charge.

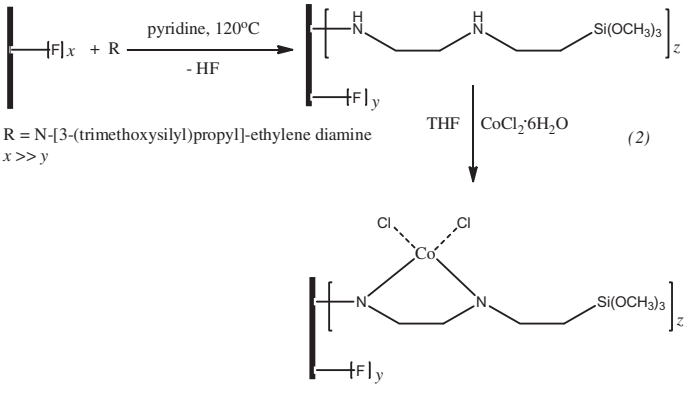

[†]Porphyrin and phthalocyanine composites with CNTs will be discussed below in separate sections.

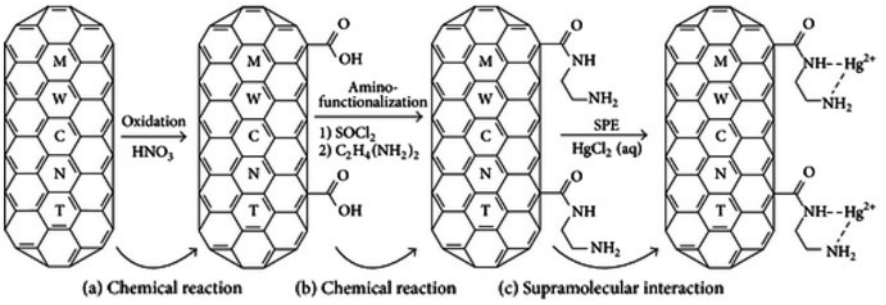

Figure 2. Schematic illustration of amino-functionalization of MWCNTs [(a) and (b)] and solid-phase extraction step (c). In the first step, MWCNTs are oxidized by HNO_3 (a) and subsequently, the oxidized MWCNTs are amino-functionalized by ethylenediamine (b). In the solid-phase extraction step, mercury ions are adsorbed on the surface of amino-functionalized MWCNTs and this is a kind of supramolecular interaction.

Ruthenium polypyridyl complexes are widely used as light harvesters in dye-sensitized solar cells. A potential application of SWCNTs is their use as active components in organic and hybrid solar cells; so, the study of the photochemistry of SWCNTs with tethered ruthenium polypyridyl complexes is important and a variety of such complexes have been obtained and studied. Among other applications of Ru/CNTs composites, we emphasize their uses as sensors. Thus, mesoporous films of platinized CNT–zirconia–Nafion composite were used for immobilization of *tris*(2,2′-bipyridyl)ruthenium(II) $\{Ru(bpy)_3^{2+}\}$ on an electrode surface to yield a solid-state electrogenerated chemiluminescence (ECL) sensor [24]. The composite films of Pt–CNT–zirconia–Nafion exhibited much larger pore diameter (3.55 nm) than that of Nafion (2.82 nm) and thus leading to much larger ECL response for tripropylamine (TPA) because of the fast diffusion of the analyte within the films. The present ECL sensor based on the Pt–CNT–zirconia–Nafion gave a linear response ($R^2 = 0.999$) for TPA concentration from 3.0 nM to 1.0 mM with a remarkable detection limit ($S/N = 3$) of 1.0 nM, which is much lower compared to those obtained with the ECL sensors based on other types of sol–gel ceramic–Nafion composite films such as silica–Nafion and titania–Nafion. In closely related research [25], an effective ECL sensor was developed by combining *bis*(2,2′-bipyridine)-5-amino-1,10-phenanthroline ruthenium(II) $[Ru(bpy)_2(5\text{-}NH_2\text{-}1,10\text{-}phen)^{2+}]$ with functionalized carbon nanotubes (FCNTs) coated on a glassy carbon electrode (figure 3). The modified electrode exhibited good electrochemical activity and ECL response. The ECL detection limit (*S/N*) for TPA using this modified electrode was 8.8×10^{-7} M L^{-1} with a linear range from 1.0×10^{-6} to 2.0×10^{-3} M L^{-1} ($R^2 = 0.9969$).

The dispersion of SWCNTs in the presence of water soluble polypyridyl complexes $[Ru_x(bpy)_yL]^{2+}$ (L = dppz **3**, dppn **4**, tpphz **5**) was achieved [26]. These ligands have extended planar π systems, which aid in the solubilization of SWCNTs via π–π interactions (composites **6–8**). Another example is a water-soluble ruthenium *tris*(bipyridyl) complex **9** linked through peptidic bonds to SWCNTs (Ru-SWCNTs) was prepared by radical addition of thiol-terminated SWCNT to a terminal C=C double bond of a bipyridyl ligand of the ruthenium *tris*(bipyridyl) complex [27]. The resulting macromolecular Ru-SWCNT (≈500 nm, 15.6% ruthenium complex content) was found to be water soluble. The emission of Ru-SWCNT was 1.6 times weaker than that of a mixture of $[Ru(bpy)_3]^{2+}$ and SWCNT of similar concentration. Time-resolved absorption optical spectroscopy allowed the detection of the $[Ru(bpy)_3]^{2+}$-excited triplet and $[Ru(bpy)_3]^{+}$.

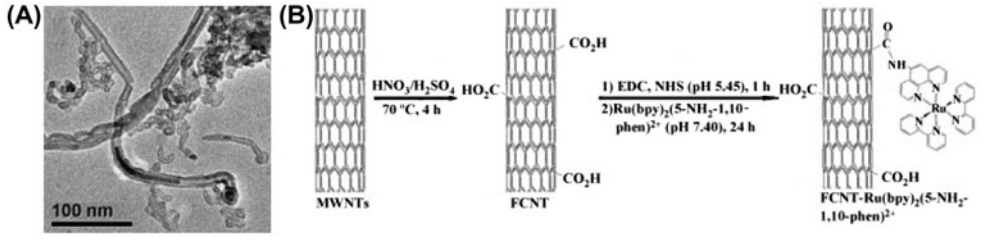

Figure 3. TEM image of FCNTs (A) and a schematic showing the steps involved in the process of combining $[Ru(bpy)_2(5\text{-}NH_2\text{-}1,10\text{-phen})]^{2+}$ with the FCNTs using the EDC and NHS linking reaction (B).

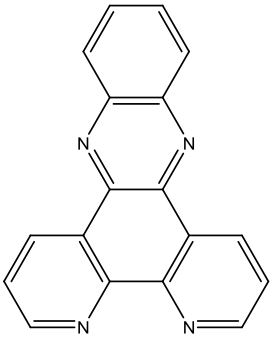

3, dppz = dipyrido[3,2-*a*:2',3'-*c*]phenazine

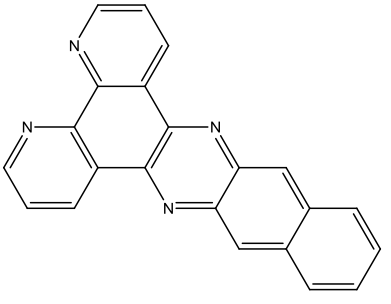

4, dppn=4,5,9,16-tetraaza-dibenzo[a,c]naphthacene, benzo[i]dipyrido[3,2-a:2',3'-c]phenazine

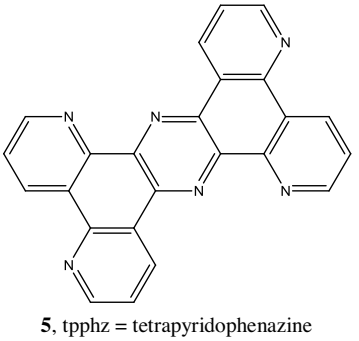

5, tpphz = tetrapyridophenazine

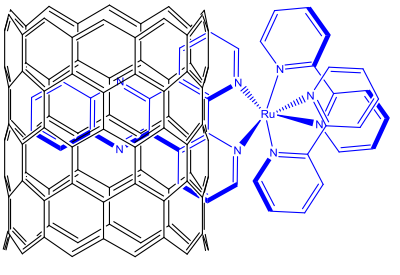

6, $[Ru(bpy)_2(dppz)]^{2+}$ composite with SWCNTs

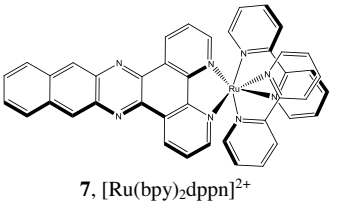

7, $[Ru(bpy)_2dppn]^{2+}$

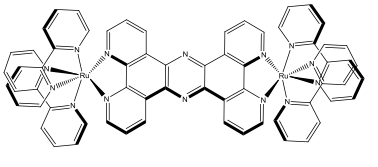

8, $[(bpy)_2Ru(tpphz)Ru(bpy)_2]^{4+}$

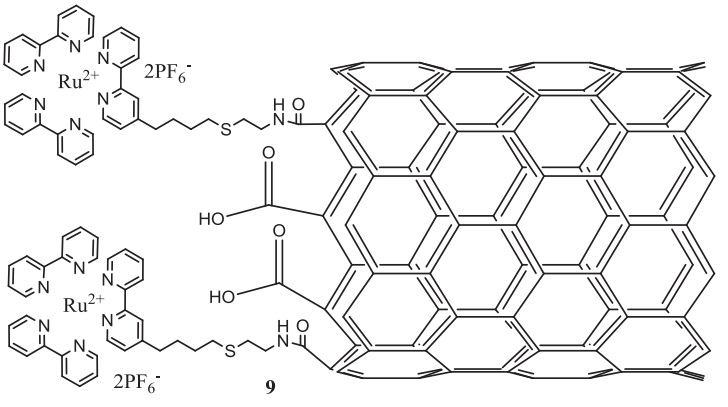

Other compounds are represented by a variety of N,O-donor ligands, classic compounds such as EDTA, salen or salophen ligands or more complex. Thus, nickel *sale*n {N,N′-*bis*(4-hydroxysalicylidene)ethylene-1,2-diamine, **10**} and *salophen* {N,N′-*bis*(4-hydroxysalicylidene)phenylene-1,2-diamine, **11**} complexes were *covalently* anchored on 20–40 nm MWCNTs (reactions *3*) [28]. Their catalytic performance for oxidation of 10 distinct primary and secondary alcohols was evaluated using periodic acid H_5IO_6 as oxidant in acetonitrile at 80 °C. The reusability of supported catalysts was investigated in the multiple sequential oxidation of benzyl alcohol, indicating excellent results. Reaction conditions were optimized for MWNT-supported salen and salophen complexes by considering the effect of parameters such as solvent, reaction time, concentration of catalyst, and amount of oxidant. The catalytic activity was higher for supported catalysts than similar homogeneous ones. These supported catalysts were stable and reused several times without loss of catalytic activity. Similar results were also reported for salen complexes with cobalt(II) [29], nickel(II) [30], and oxovanadium(IV) [31]. In the last case, liquid-phase oxidation of cyclohexane with H_2O_2 to a mixture of cyclohexanone, cyclohexanol, and cyclohexane-1,2-diol in CH_3CN was reported using oxovanadium(IV) Schiff-base complex **12** covalently anchored on modified MWNTs as catalysts.

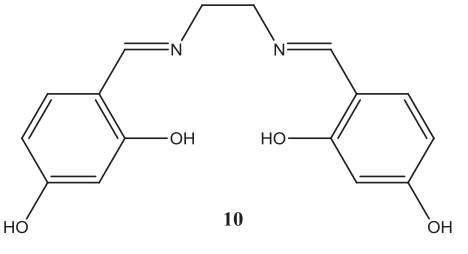

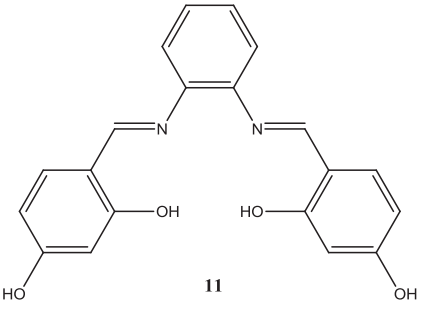

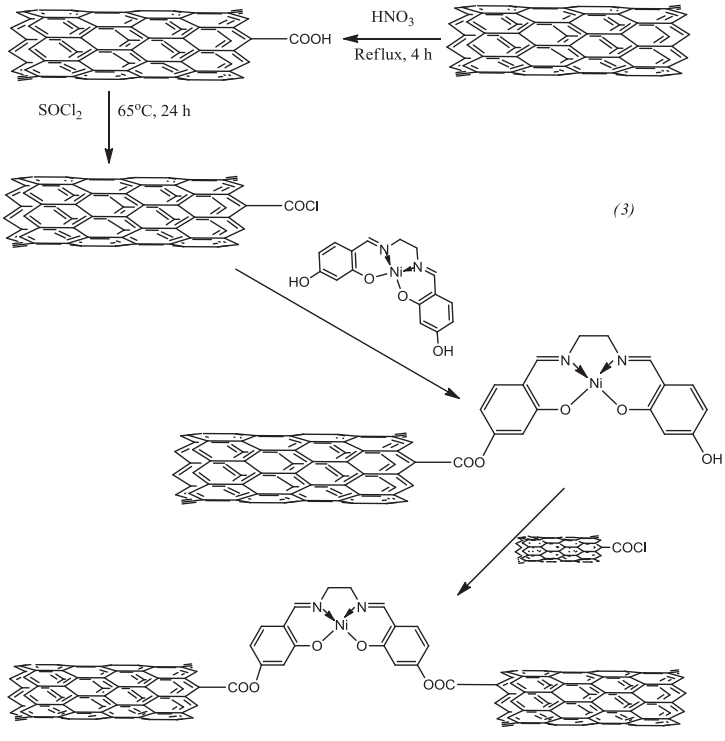

Synthesis of MWNT-supported nickel complexes.

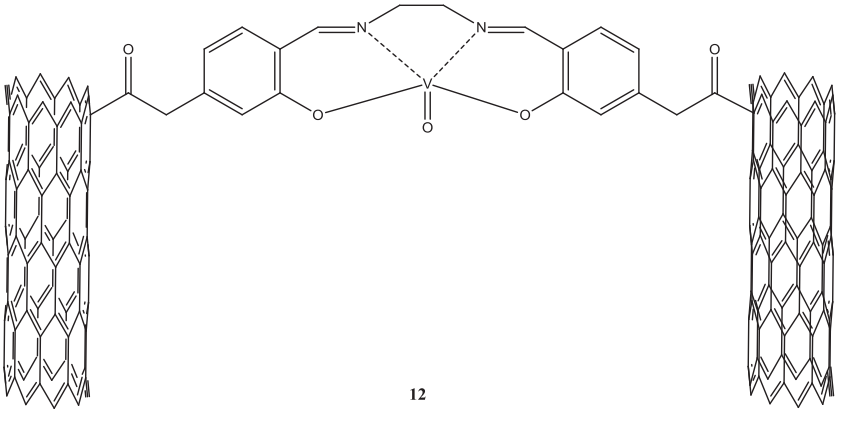

12

Related Cu_2 bisalophen complex **13** can be assembled in a *non-covalent* manner (figure 4) on SWNTs elaborated by HiPCO and hot filament-assisted chemical vapor deposition techniques [32]. The origin of the nanotubes seems to not affect the electronic interaction responsible for this assembly. Non-covalent grafting of transition metal complexes onto SWNTs in a CNFET channel leads to electron transfer from the molecules to the nanotube and generates a tunable ambipolar effect in ambient air. This opens the possibility to design new kinds of nanohybrid circuits. In addition, the MWCNTs-palladium(II)-Schiff base

complex (for the synthesis, see reaction scheme *4*) efficiently catalyzed the coupling reactions of acid chlorides with terminal alkynes under copper-, phosphorous-, and solvent-free conditions in air (reaction *5*) for the synthesis of α, β-acetylenic ketones under aerobic conditions. This moisture and air stable heterogeneous catalyst could be simply recovered and used in four successive runs [33].

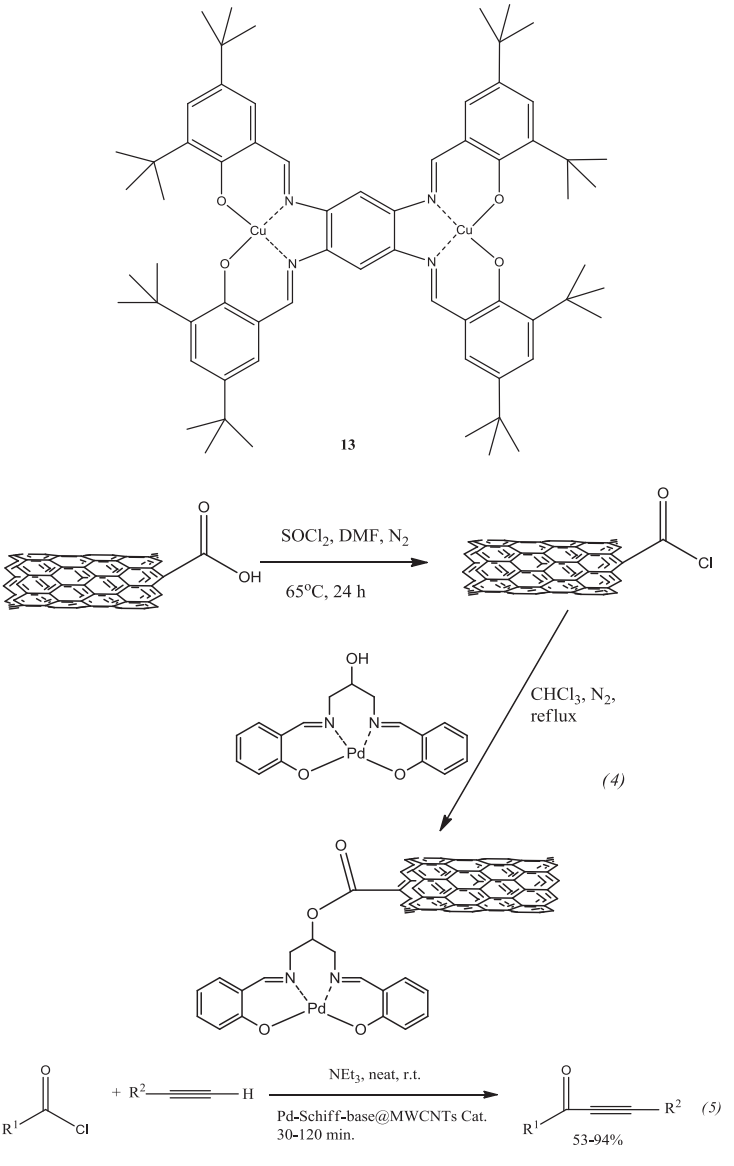

An interesting functionalization method for SWCNTs was offered [34]. Cu^{2+} was effectively coordinated with a SWCNT to produce a SWCNT–Cu^{2+} complex by a metal coordination reaction in ultrasonic conditions. Since the complex was very reactive towards the carboxylic acid group, the chemical functionalization of SWCNTs was easy to accom-

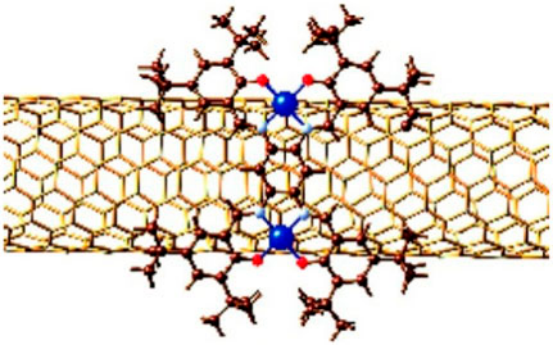

Figure 4. View of the optimized structure (perpendicular orientation for **13** grafted onto a (7,6) nanotube from theoretical calculations). Blue, red, light blue, and brown spheres correspond to copper, oxygen, nitrogen, and carbon, respectively; hydrogens are indicated as brown sticks (see http://dx.doi.org/10.1080/00958972.2014.888063 for color version).

plish. This approach was used to functionalize the surface of the SWCNTs with stearic acid (SA) or EDTA (figure 5) for tuning of the relative hydrophobicity and hydrophilicity of the surface, respectively. Functionalization of SWCNTs by metal coordination reaction effectively modified the SWCNT surface, while conserving the excellent physical properties of the SWCNTs. The surface properties of the SWCNTs were easily tuned by introduction of the functional groups required for specific applications. Using the EDTA analog, DETPA (diethylenetriaminepentaacetic acid **14**), by combining the electrostatic interaction between the Fe^{III}-DETPA complex and polyallylamine (PAH) functionalized MWCNTs as well as the ionotropic cross-linking interaction between PAH and ethylenediamine-tetramethylene phosphonic acid (EDTMP **15**), the electroactive Fe^{III}-DETPA complex was incorporated within the MWCNT matrix, and firmly immobilized on the Au substrate electrode [35]. The influences of solution pH and ionic strength on this electrochemical sensor were investigated, showing that the sensor had a fast response to hydrogen peroxide (<3 s) and an excellent linear range of concentration from 1.25×10^{-8} to 4.75×10^{-3} M with a detection limit of 6.3×10^{-9} M under the optimum conditions.

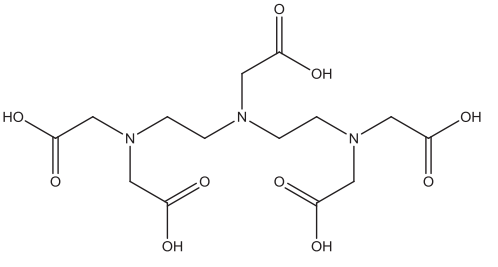

14 DETPA

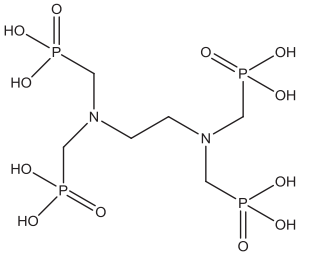

15 EDTMP

Studies on covalent chemical functionalization of SWCNTs with polynuclear $\{Mn_4\}$ coordination complexes showed that the reaction can only be achieved for tubes which were oxidized to create carboxylic groups [36]. Further functionalization of CNT-COOH was carried out by the ligand exchange reaction (*6*) $\{H_2L = 2,6\text{-}bis(1\text{-}(2\text{-hydroxyphenyl})$

iminoethyl)-pyridine}. The choice of the $\{Mn_4\}$ complexes was motivated by the fact that they feature four replaceable carboxylate groups, while two additional multidentate pyridine-based ligands remain strongly coordinated and retain the central Mn_4O_4 cubane core structure. The reaction is based on ligand exchange between the ligands of the complex and the carboxylic groups created on the CNTs by oxidation in air. In addition, an amperometric biosensor for catechol, based on immobilization of a highly sensitive horseradish peroxidase by affinity interactions on metal chelate-functionalized agarose/CNTs composites, was created [37]. Metal chelate affinity takes advantage of the affinity of Ni^{2+} ions to bind strongly and reversibly to histidine or cysteine tails found on the surface of the horseradish peroxidase (reactions *7*). Thus, enzymes with such residues in their molecules can be easily attached to functionalized agarose/CNT composites containing a nickel chelate. Catechol was determined by direct reduction of biocatalytically liberated quinone species at −0.05 V (*versus* SCE). The performance of the proposed biosensor was tested using four different phenolic compounds, showing very high sensitivity, in particular, the linearity of catechol is observed from 2.0×10^{-8} to 1.05×10^{-5} M with a detection limit of 5.0×10^{-9} M. Metal ions were compared between Ni^{2+}, Co^{2+}, Fe^{2+}, Cu^{2+}, Fe^{3+}, Ca^{2+}, Mg^{2+}, and Al^{3+}. The maximum response current of the biosensor was attained for Ni^{2+}, because Ni^{2+} ions possess coordination numbers of six, and the quadridentate epichlorohydrin occupies three coordination positions, leaving three positions available for strong but reversible interactions with proteins.

$$CNT{-}COOH + [Mn_4L_2(CH_3COO)_4] = CNT{-}COO - [Mn_4L_2(CH_3COO)_3] + CH_3COOH \quad (6)$$

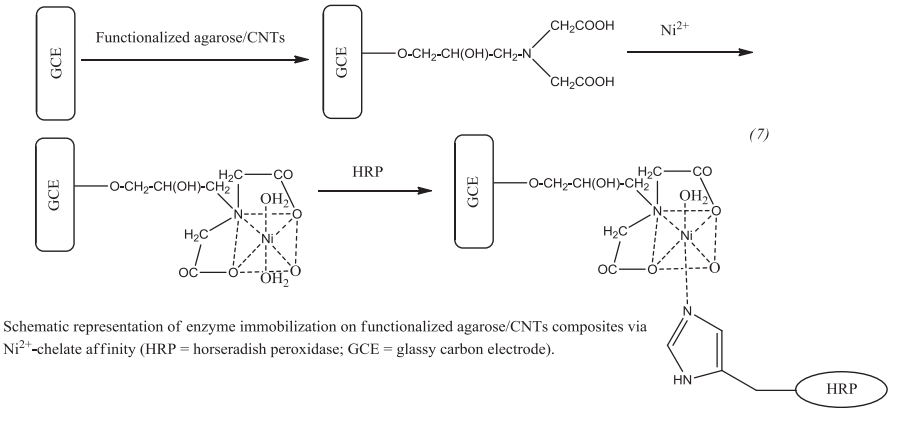

Schematic representation of enzyme immobilization on functionalized agarose/CNTs composites via Ni^{2+}-chelate affinity (HRP = horseradish peroxidase; GCE = glassy carbon electrode).

Three hybrid materials, synthesized [38] with *N*-(2-vinylsulfanyl-ethylidene)-benzene-1,2-dimine (**16**, SBD), *N*-pyridin-2-ylmethylene-benzene-1,2-dimine (**17**, NBD), and *N*-furan-2-ylmethylene-benzene-1,2-dimine (**18**, OBD), covalently linking to MWCNTs (reaction scheme *8*), were used both as ionophores and as ion–electron transducers to construct Ag^+ carbon paste electrodes. The resulting electrodes showed higher selectivity to Ag^+ than other cations tested; among the three electrodes, the electrode based on SBD-g-MWCNTs with optimum composition showed the best performance to Ag^+.

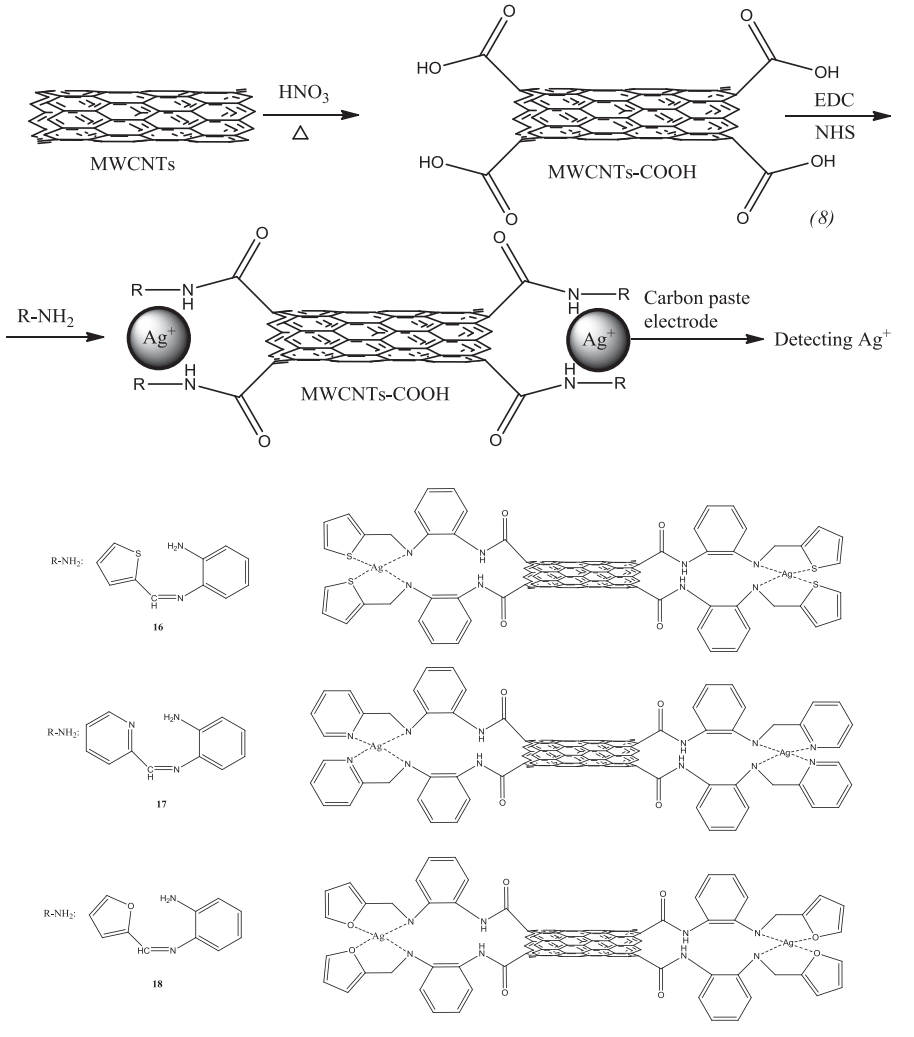

Schematic representation of the synthetic procedure for three MWCNT hybrids.

Porphyrin-functionalized CNTs

Both free porphyrins [39] and their metal complexes [40] have been applied for functionalization of CNTs (mainly SWCNTs), frequently in combination with fullerenes [41]. As an example of a non-metal porphyrin functionalization of CNTs, SWCNTs were modified with porphyrin units [42] with aid of two strategies. In the first approach, the electropolymerization of pyrrole or pyrrole-substituted porphyrin monomers occurred via formation of conjugated positively charged polypyrrole (PPyrr) backbone, while negatively charged CNTs functionalized with carboxylic groups (SWCNT-COOH) acted as a polymer dopant. In the second case, the SWCNT–porphyrin composites were chemically synthesized

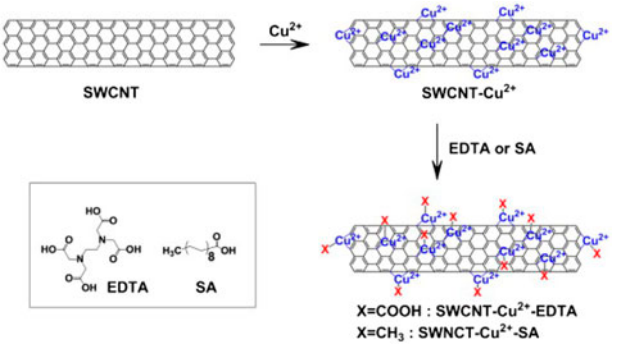

Figure 5. Procedures for the metallization of SWCNTs with Cu^{2+} ions by the metal coordination reaction and for the subsequent surface modification of SWCNTs with carboxylic acid and methyl groups by coordination between the Cu^{2+} and EDTA or SA, respectively. X in the final products, SWCNT–Cu^{2+}–EDTA or SA represents functional group terminated on SWCNT surfaces after coordination reaction between SWCNT–Cu^{2+} and EDTA or SA.

via interaction between glycyl-substituted porphyrin and non-modified CNTs and then entrapped in PPyrr/SWCNT-COOH film.

Several metal porphyrins, most frequently those of zinc, iron, and ruthenium, were used for CNTs functionalization. Thus, dispersible SWCNTs grafted with poly(4-vinylpyridine), SWCNT-PVP, were tested in coordination assays with zinc tetraphenylporphyrin {Zn(TPP)} (TPP = tetraphenyl porphyrin **19**), showing the formation of a SWNT-PVP·Zn(TPP) nanohybrid **20** (reaction *9*) [43]. Temperature can be used to control the SWNT-PVP·Zn(TPP) association; the SWNT-PVP coordination to ZnP was labile and dynamic. Hence, increasing or decreasing the temperature weakens or strengthens the complex, respectively. In this context, fluorescence emerged as a sensitive temperature probe. Temperature increase, for example, led to a notable reactivation of the ZnP fluorescence, while lower temperatures essentially caused deactivation. Porphyrins and their zinc complexes can be used to solubilize CNTs in water. The porphyrins used for the solubilization of CNTs are usually TPP analogs. However, TPP analogs do not favor the formation of π–π interactions because the aryl groups prevent the porphyrin moiety from approaching the CNT surface due to the perpendicular conformation of the porphyrin moiety and its aryl group substituents. To avoid this, non-TPP-type porphyrins **21**, with chiral and hydrophilic substituents, that make the porphyrins soluble in water, were synthesized [44]. SWNTs were effectively dissolved into water by the non-TPP type chiral porphyrins, and the dissolved chiral porphyrin/SWNTs composites could be easily redissolved. Both the dissolved and redissolved SWNT solutions were very stable and did not form apparent aggregates even after being kept for six months.

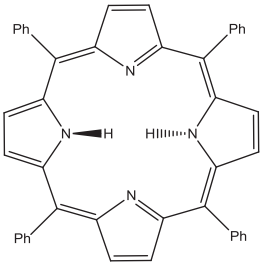

TPP

19

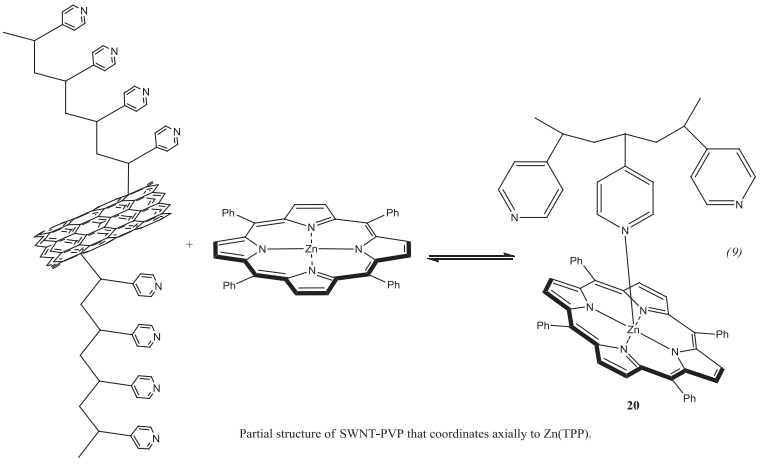

Partial structure of SWNT-PVP that coordinates axially to Zn(TPP).

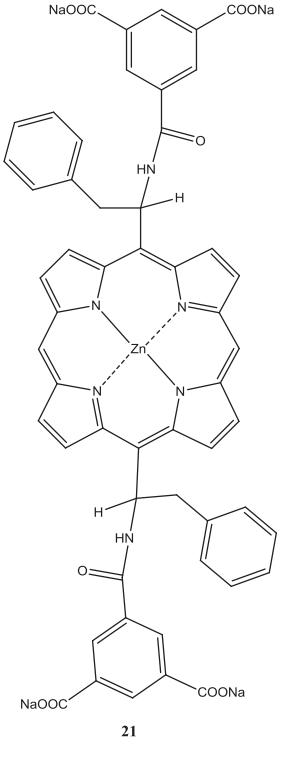

(R)- and (S)-5,15-*bis*(1-(1′,3′-isophthalic acid disodium salt-5′-carbamoyl)-2-phenyl-ethyl)porphyrin Zn(II).

Covalent and non-covalent attachment of an iron porphyrin FeP on different surfaces of SWCNTs (figure 6) were studied by density-functional theory calculations and molecular dynamic simulations [45]. Two mechanisms for the FeP attachment on metallic and semiconducting CNTs were considered, by physisorption through π–π-stacking interaction

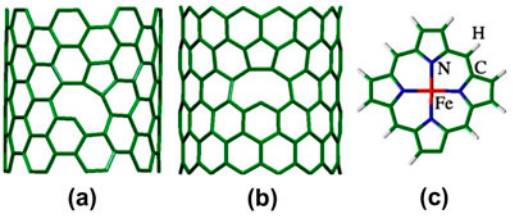

Figure 6. Equilibrium geometries of CNTs with a single vacancy: (a) (8,8)+V, (b) (14,0)+V, and (c) the FeP radical with a missing H atom (FeP*).

and by chemisorption through sp^2 and sp^3 bonding configurations. Figure 7 shows the results for the equilibrium geometries of FeP attached on pristine (8,8) CNT by physisorption [figure 7(a)], and FeP* (FeP radical, formed by removing a H atom from FeP to allow formation of a sp^3-like C–C bond between the CNT and the FeP radical) attached on both pristine (8,8) and defective (8,8)+V CNTs by chemisorption [figure 7(b) and 7(c), respectively]. The authors concluded that FeP covalently linked to metallic CNTs would be the best electrocatalytic system due to its metallic character at r.t., suggesting that they may work as an electrode with the ability to transport charge to the macrocycle. Semiconducting CNTs would be unlikely because the FeP-CNT assembly preserves the semiconducting character. Non-covalent attachment of FeP onto both CNTs was proposed to be also unlikely due to the absence of physical contact and the unsuccessful FeP fixation.

In addition to ruthenium polypyridyl complexes described above, ruthenium porphyrin-functionalized SWCNTs arrays (figure 8) were prepared using coordination of the axial position of the metal ion onto 4-aminopyridine preassembled SWCNTs directly anchored to a silicon(100) surface (SWCNTs-Si) [46]. Mixed assembly of ferrocene/porphyrin onto CNT arrays was achieved (figure 9) by altering the ratio of two redox-active species in the deposition solution. These ruthenium porphyrin modified electrodes are excellent

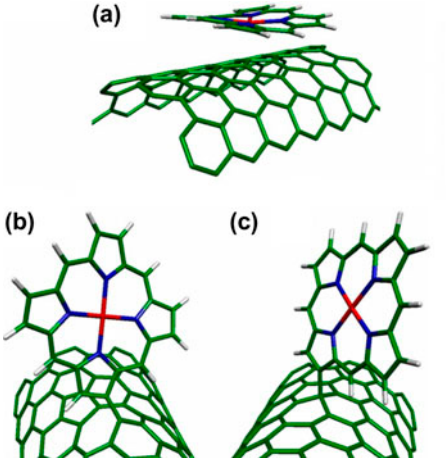

Figure 7. Equilibrium geometries of FeP and FeP* adsorbed on the metallic (8,8) CNT. (a) FeP physisorption on the perfect CNT; (b) FeP* chemisorption on the defective (8,8)+V CNT by sp^2 bonding; and (c) FeP* chemisorption on the perfect CNT by sp^3 bonding.

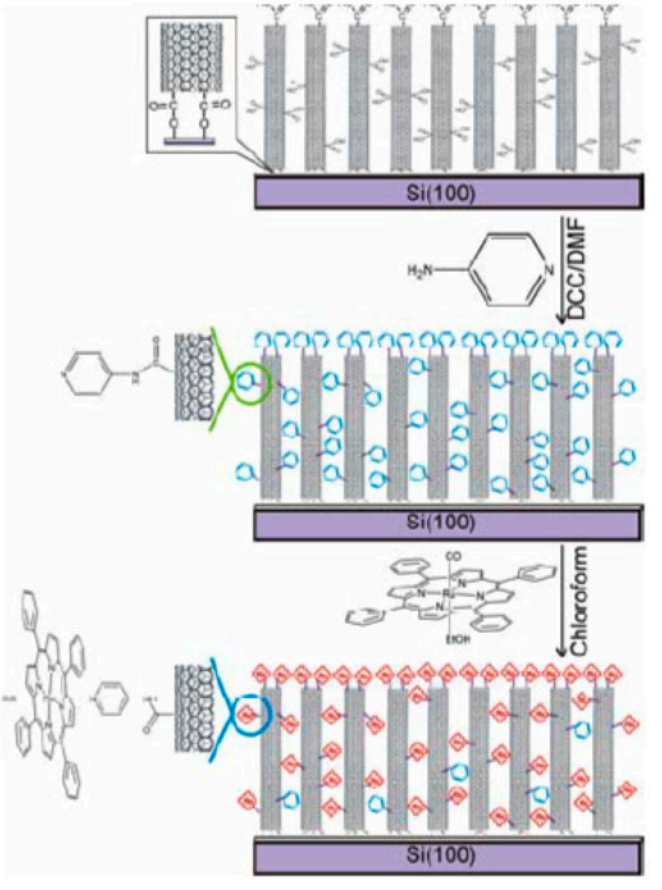

Figure 8. Schematic representation of the preparation of RuTPP-SWCNTs-Si.

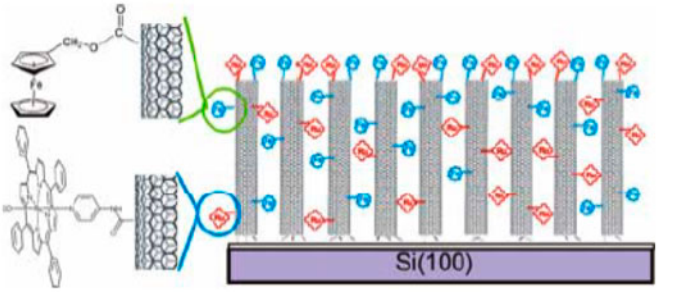

Figure 9. Mixed assembly of ferrocene/porphyrin onto carbon nanotube arrays.

candidates for molecular memory devices. Also, a dihydroxotin(IV) porphyrin-functionalized SWNTs nanohybrid (figure 10) was obtained [47]. The structural design of this tin porphyrin was based on three considerations: (1) the OH axial ligands of the tin porphyrins

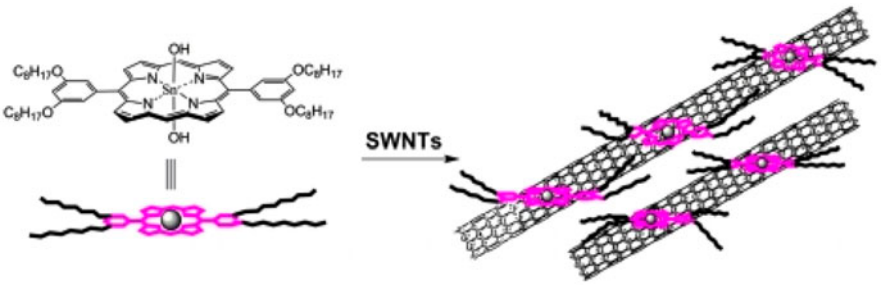

Figure 10. Schematic view of the Sn(IV) porphyrin-functionalized SWNTs.

can be displaced easily by carboxylate and phenoxide. There are large numbers of COOH, OH groups on both the sidewalls and the ends of the nanotubes after acid treatment of SWNTs, which could react with the axial OH of the tin porphyrin; (2) long alkyl chains will increase solubility of SWNTs in organic solvents and stabilize SWNTs dispersion; and (3) ^{119}Sn NMR can be used to further explore the interaction between SWNTs and the functional groups, which is difficult in most other cases for SWNT materials. It was demonstrated that efficient electron transfer occurs within the nanohybrid at the photoexcited state and the charge-separated state of the nanohybrid was observed by transient absorption spectrum. The product possesses solubility in a series of organic solvents, for instance (mg/L, r.t.): in 1,2-dichlorobenzene 440, chloroform 358, toluene 237, and tetrahydrofuran 209, in hexane, ethanol, and methanol – <1 mg L^{-1} under sonication for over 2 h. This soluble electron donor–acceptor nanohybrid might be a good candidate as a light harvesting material in molecular photoelectronic devices.

In addition to existing porphyrin-CNT hybrids, we emphasize investigations of *porphyrin-like defects* in CNTs surface, which have important applications. Thus, systemic study of the chemical functionalization of (10,0) SWCNT doped with porphyrin-like nitrogen defects (4ND-CNxNT) with 10 different transition metals (TMs=Sc, Ti, V, Cr, Mn, Fe, Co, Ni, Cu, and Zn) defined as TM/4ND-CNXNT (figure 11) was done with the spin-unre-

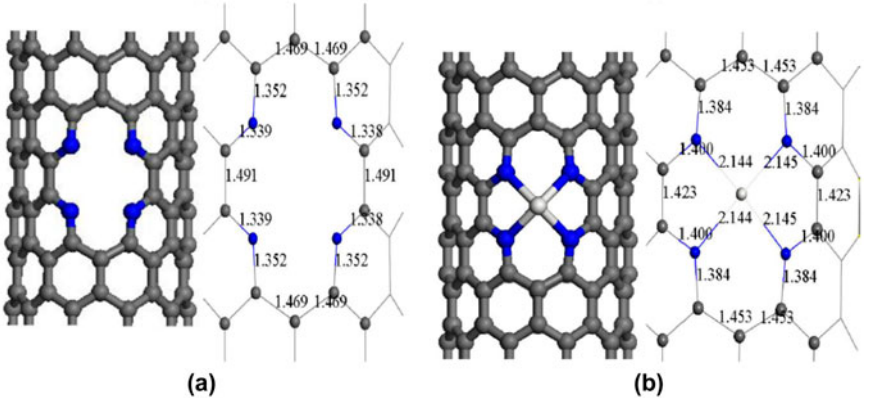

Figure 11. Optimized geometry of (a) the infinite (10,0) zigzag SWCNT with porphyrin defects (4ND-CNxNT) and (b) 4ND-CNxNT functionalized with TM. Gray color depicts carbon atoms; blue is nitrogen, and white is TM, in this case Scandium (see http://dx.doi.org/10.1080/00958972.2014.888063 for color version).

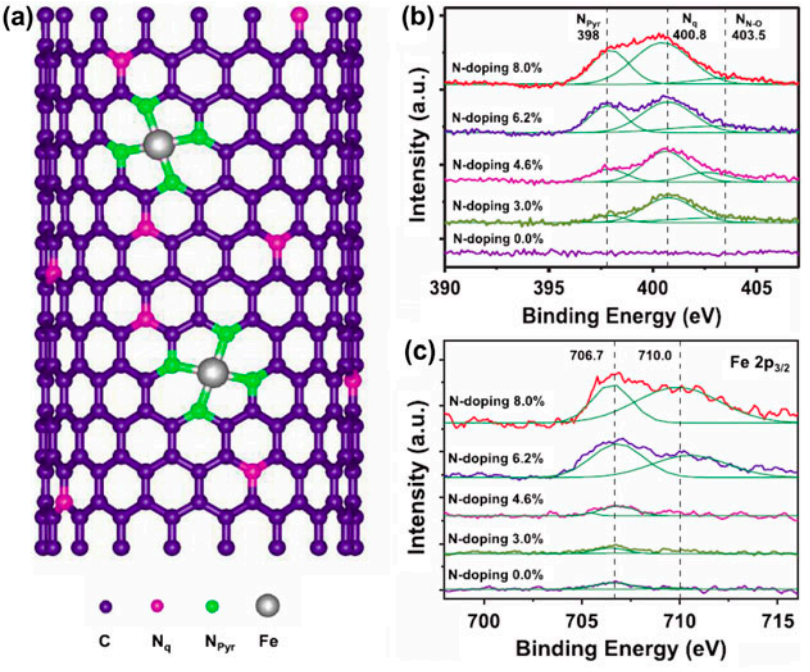

Figure 12. (a) Schematic illustration of the Fe-Por CNT. The blue, magenta, green, and gray spheres indicate the C, quaternary N (N_q), pyridinic N (N_{Pyr}), and Fe atoms, respectively. XPS spectra of (b) N and (c) Fe for the as-grown CNTs with doping levels of 0.0–8.0%. The N 1s peak is deconvoluted into three peaks at 398 (N_{Pyr}), 400.8 (N_q), and 403.5 eV (N_{N-O}). The Fe $2p_{3/2}$ peak is deconvoluted into two major peaks at 706.7 and 710.0 eV (see http://dx.doi.org/10.1080/00958972.2014.888063 for color version).

stricted DFT method [48]. The composite material TM/4ND-CNXNT showed very strong binding to hydrogen and can act as a media for storing hydrogen. Another example is a Fe-porphyrin-like CNT, fabricated by conventional plasma-enhanced CVD in NH_3 using highly uniform nanopatterned Fe particles (≈13 nm diameter, ≈36 nm center–center distance) on a silicon substrate resulted in covalent, seamless incorporation of the 5-6-5-6 porphyrinic Fe–N_4 moiety into the graphene hexagonal side wall [49]. *N*-doping levels were 0–8.0% (figure 12). The resulting biomimetic nanotube exhibited excellent oxygen reduction catalytic activity. This non-Pt catalyst would directly impact on proton exchange membrane and direct methanol fuel cell technologies in terms of performance, material cost, and stability.

Phthalocyanine-functionalized CNTs

As for porphyrins, both free phthalocyanines and their metal complexes have been applied for functionalization of CNTs via covalent or non-covalent interactions. Thus, the covalently bonded phthalocyanine conjugates **22–23** with fluorinated F-SWCNTs were synthesized [50]. Their thermal decomposition corresponds to the destructive fragmentation of peripheral phthalocyanine substituents as the first stage of the process followed by degradation of macrocycles at the last decomposing stage. The mass loss at 400–600 °C is characteristic for CNTs.

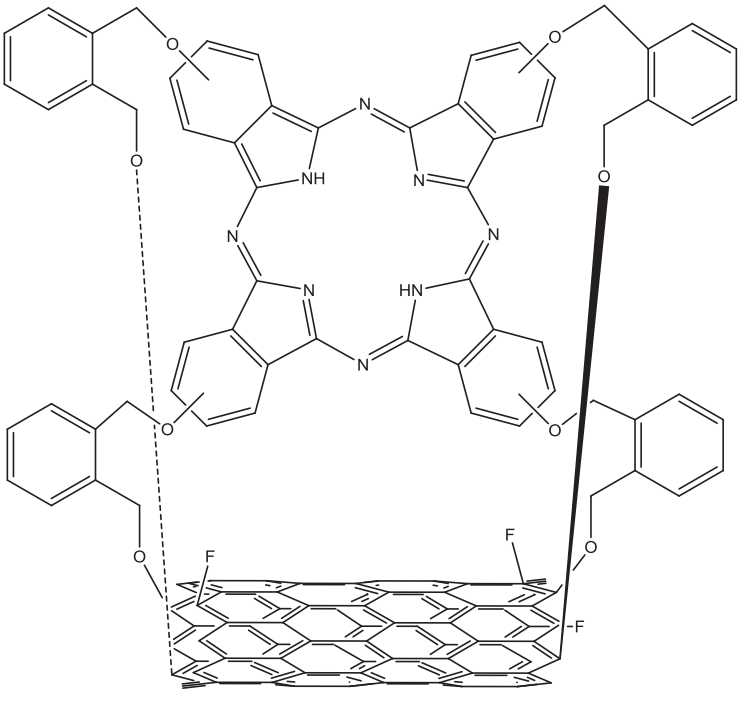

22 F-SWCNT

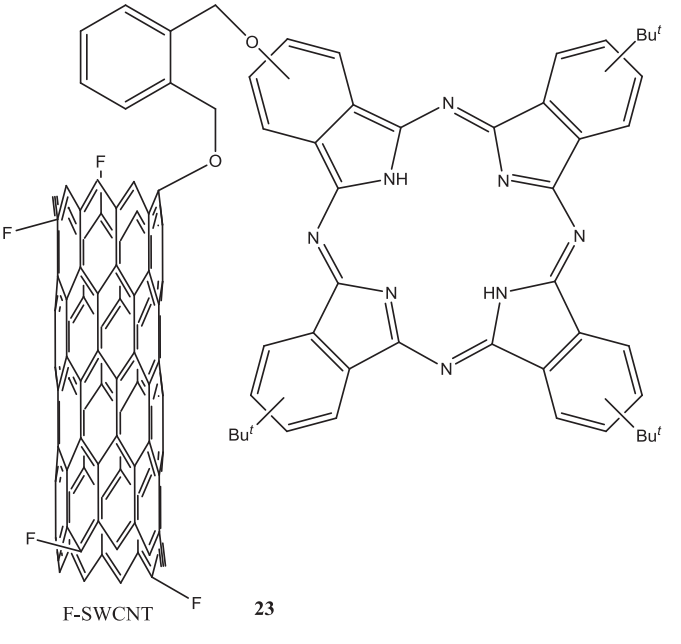

F-SWCNT **23**

Several classic metal phthalocyanines {M is generally transition metal (Fe, Co, Cu, Mn) or zinc} have been applied for CNT functionalization. Thus, metal (M=Fe, Co) phthalocyanine and porphyrin-functionalized MWCNTs were used as non-precious electrocatalysts for the

electroreduction of oxygen [51, 52]. To adsorb the metal macrocyclic catalyst on the surface of MWCNTs, a mixture of FePc, CoPc, FePh or CoPh, and MWCNTs in isopropanol was prepared in sonication conditions and further heating at 400 and 800 °C before electrochemical testing. It was found that metal-porphyrin-based electrodes heat-treated at 800 °C possessed higher O_2 reduction activity than metal-phthalocyanine catalysts. The authors proposed that pyridinic-type nitrogen, forming at temperatures as high as 800 °C, could be responsible for the catalytic activity.

Covalent functionalizations of metallic CNTs with transition metal phthalocyanines (MPc, with M=Mn, Fe, and Co) were studied by DFT calculations [53]. The CNT–MPc catalytic activity toward oxygen reduction (ORR) was investigated through the O_2 stretching frequency adsorbed on the phthalocyanine metal center (figure 13). Better reduction abilities were found when the CNT functionalization occurs through sp^2-like bonds. In contrast, weaker sp^3 functionalization showed ORR activity close to those found for the isolated macrocycles. Multiple stable-spin states for the M–O_2 adduct were also found for M=Mn and Fe, suggesting higher ORR rates. The phthalocyanine metal center catalytic activity increases following the order: Mn > Fe > Co. In a related report [54], amino-functionalized a-MWCNTs-supported iron phthalocyanine (FePc) (a-MWCNT/FePc) was investigated as a catalyst for ORR in an air–cathode single-chambered microbial fuel cell (MFC), providing a potential alternative to Pt in MFCs for sustainable energy generation. In addition, FePc coated on

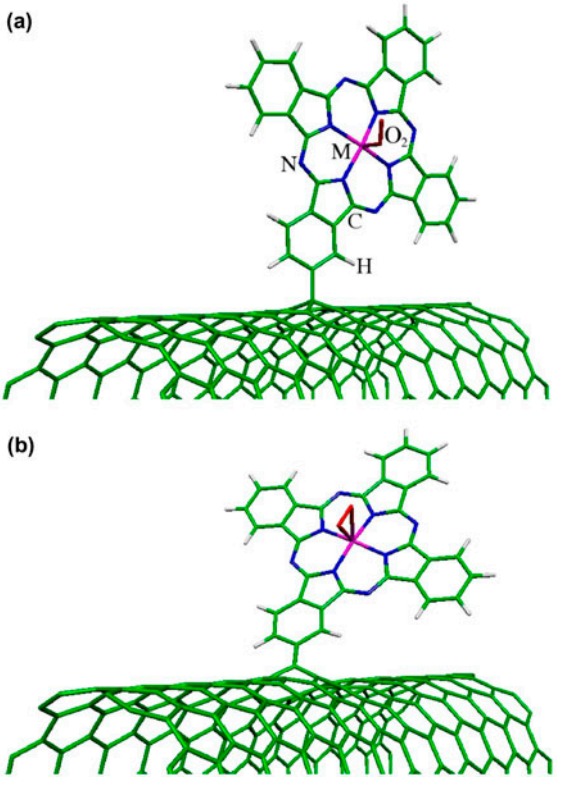

Figure 13. Stable geometries of the O_2 molecule adsorbed on the phthalocyanine metal center of the CNT–MPc complex. (a) CNT–MPc in the sp^3 bonding structure and M–O_2 adduct in the end-on geometry. (b) CNT–MPc in the sp^2 bonding structure and M–O_2 adduct in the side-on geometry.

SWCNTs, synthesized as a non-noble electrocatalyst for the ORR, exhibited higher activity than the commercial Pt/C catalyst, and excellent anti-crossover effect for methanol oxidation in the ORR [55].

Several examples of non-covalent functionalization are also known for phthalocyanine-CNT composites. Thus, studies of a hybrid material composed of SWNTs and cobalt phthalocyanine (CoPc) derivatives **24** revealed [56] that the CoPc derivatives were anchored on the surface of nanotubes through π–π stacking. Gas sensor tests were performed to check the potential of this hybrid material while sensing devices were fabricated. The synergetic behavior between both of the candidates allowed excellent sensitivity and selectivity to dimethyl methylphosphonate (DMMP) (stimulant of nerve agent sarin). Also, MWCNTs were non-covalently functionalized with different metal (M=Zn, Cu, Ni) phthalocyanines by π–π stacking [57] via dispersion by sonication into the phthalocyanines solution in chloroform or DMF before purification by centrifugation. The metal phthalocyanine molecules adhered to the surface of MWCNTs in the TEM images.

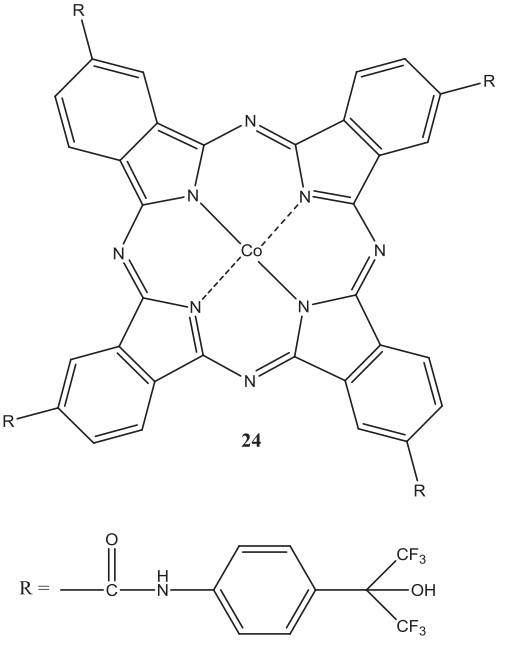

A family of pyrene **25** (Pyr)-substituted phthalocyanines (Pcs) (see also the detailed pyrene section below), i.e. ZnPc-Pyr and H_2Pc-Pyr, were designed, synthesized (reaction scheme *10*), and probed in light of their spectroscopic properties as well as their interactions with SWNTs [58]. Owing to the ability of pyrene to adhere to SWNT sidewalls by π–π interactions, this polyaromatic anchor was exploited to immobilize metal-free (H_2Pc) as well as zinc (ZnPc) phthalocyanines onto the surface of SWNTs. The pyrene units provided the means for non-covalent functionalization of SWNTs via $\pi-\pi$ interactions, ensuring that the electronic properties of SWNTs are not impacted by chemical modification of the carbon skeleton. Transient absorption experiments reveal photoinduced electron transfer between the photoactive components. ZnPc-Pyr/SWNT and H_2Pc-Pyr/SWNT have been integrated into photoactive electrodes, revealing stable and reproducible photocurrents with monochromatic internal photoconversion efficiency values for H_2Pc-Pyr/SWNT as large as 15 and 23% without and

with an applied bias of +0.1 V. Related zinc monoamino phthalocyanine ZnMAPc–pyrene complex and its hybrid with SWCNTs was also described [59].

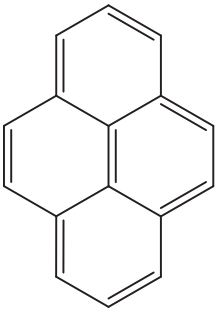

25

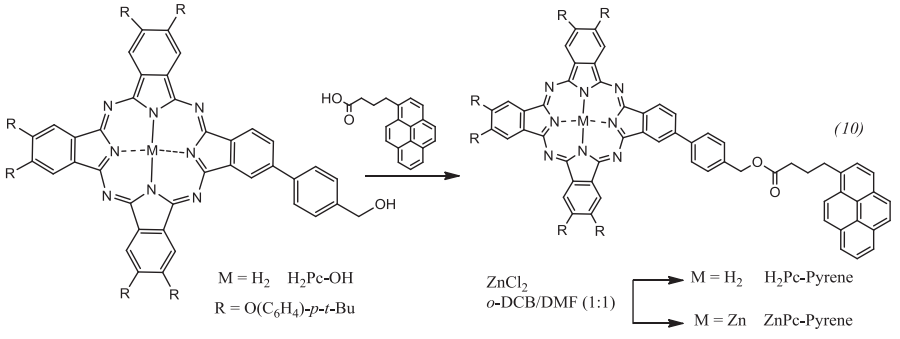

Composites of CNTs with complexes of sulfur-containing ligands

Sulfur-containing ligands are practically absent. The only exception is the synthesis and structural characterization of a stable discrete *bis*-dithiolene complex, $[PPh_4][Cu(DMED)_2]$ (DMED = 1,2-dicarbomethoxy-1,2-dithiolate), involving the reaction between a copper polysulfide precursor with activated acetylene, was reported [60]. This complex, possessing terminal –CO-OCH_3 groups, forms nanospheres by hydrogen bonding in a mixture of solvents containing water as one of the components. These nanospheres further aggregate with water soluble (carboxylated) carbon nanotubes (wsCNTs). These nano-composites are assisted by hydrogen bonding between carboxylic acid groups of the wsCNTs and the peripheral–$COOCH_3$ groups of the coordinated dithiolenes of the nanospheres, which is promoted by water.

Functionalization of CNTs with organometallics

Metal cyclopentadienyls

A simple method for tuning catalytic property of a classic widely used metallocene-based catalyst, Cp_2ZrCl_2, for ethylene polymerization by the direct adsorption (figure 14) of Cp_2ZrCl_2 onto MWCNTs was reported as far back as in 2006 [61]. Direct interactions between MWCNTs and Cp rings of Cp_2ZrCl_2 controlled the polymerization behaviors, and the polyethylene with an extremely high molecular weight (MW = 1,000,000) can be thus

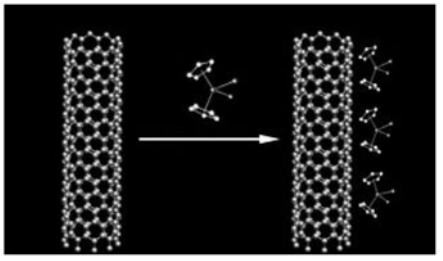

Figure 14. Preparation of Cp_2ZrCl_2–MWCNT.

generated. Also, SWNTs and MWNTs were covalently functionalized with a titanium alkoxide catalyst through a *Diels-Alder* cycloaddition reaction (reaction scheme *11*) [62] and used for the surface initiated titanium-mediated coordination polymerizations of L-lactide, ε-caprolactone, and *n*-hexyl isocyanate employing the "grafting from" technique. The final polymer-grafted CNTs were readily dissolved in organic solvents as compared to the insoluble pristine and catalyst-functionalized CNTs. In addition, the interaction of organometallic chromium-centered free radicals generated by the homolytic dissociation of (pentamethylcyclopentadienyl)-chromiumtricarbonyl dimer $[Cp^*Cr(CO)_3]_2$ {forming $^*Cp{\cdot}Cr(CO)_3$} in toluene with SWNTs was investigated [63]. Chromium-centered free radicals were added to the surface of nanotubes through oxygens than to sidewall carbons. It was concluded that chromium in the $^*Cp{\cdot}Cr(CO)_3$ free radical attacks irreversibly oxygens in the oxidized nanotube with substantial transfer of electron density from chromium to oxygen. It was also shown that chromium-centered free radicals interact preferentially with SWNT of smaller diameter; addition of chromium-centered radicals to SWNT resulted in partial changes in the electronic structure of nanotubes. The observed sidewall-functionalized CNTs involving addition of chromium complex can be useful for the development of new supported catalysts with interesting catalytic properties.

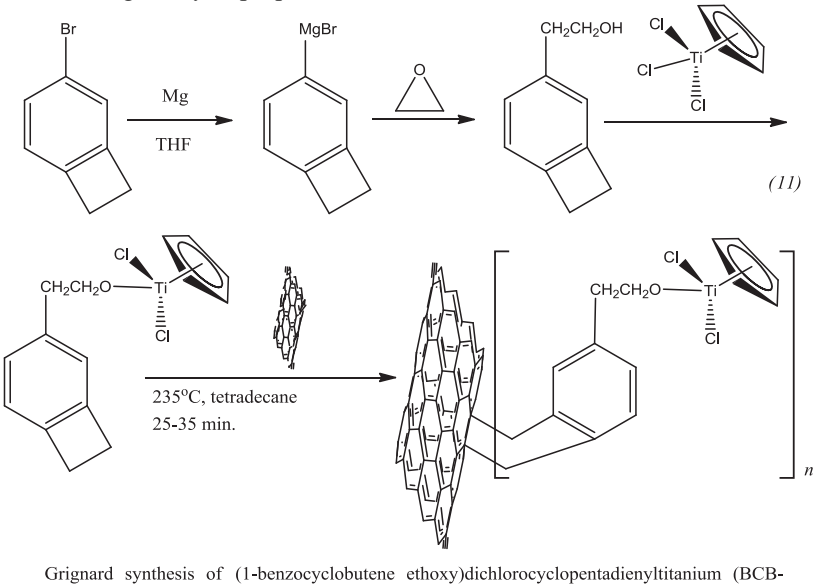

Grignard synthesis of (1-benzocyclobutene ethoxy)dichlorocyclopentadienyltitanium (BCB-EOTiCpCl$_2$) and covalent functionalization of MWNTs using a [4+2] *Diels-Alder* cycloaddition reaction.

A theoretical characterization of transition metal cyclopentadienyls (CpM, M=Fe, Ni, Co, Cr, Cu) adsorbed on pristine and boron-doped carbon nanotubes (B-CNTs) and boron-doped graphenes was carried out using spin-polarized DFT calculations (figure 15) [64]. Significant increase of the binding energies between CpTM and boron-doped CNTs and graphenes (*versus* pristine carbon supports), surpassing even the adsorption strength of the isolated metals (by about 2 eV), were revealed. Both the delocalization of the metal *d*-state by the presence of the Cp ring and the π-stacking interactions between the Cp ring and the carbon substrate are responsible for enhancement of the binding energies. This stabilization may play an important role in immobilizing ferrocene-based catalysts. The following characteristics, with some exceptions, were observed for the CpM adsorption: (a) most CpM complexes occupy the hollow sites of the six-member ring center and (b) some complexes adsorb near the center on the sidewall.

Ferrocene-functionalized [65] CNTs are the object of a series of recent reports; their interaction could be *covalent, non-covalent, or both* at the same time. Thus, a ferrocene-functionalized SWCNT *non-covalent* nanohybrid was investigated by using a ferrocene/SWCNT interdigitated construction film as an electrode for L-glutamate detection {exhibiting high catalytic efficiency, high sensitivity, and fast response during the detection of a low concentration of L-glutamate (1 μM)} [66]. Ferrocene could immobilize on the surface of SWCNT bundles, and the ferrocene/SWCNT hybrid had high stability not only in water but also in ethanol and acetone (no sediment was observed for more than three months). Unlike the previous example, *covalent* functionalization (figure 16) of few-wall CNTs (FWCNTs) by ferrocene derivatives improved their dispersion efficiency in water and allowed graft electroactive chemical groups on their side-walls to promote electron transfer to biomolecules [67]. Thus, functionalized CNTs (f-CNTs) were used to modify a glassy carbon electrode and this modified electrode was applied for oxidizing the cofactor NADH (dihydronicotinamide adenine dinucleotide). Shortened and oxidized MWCNTs were also functionalized with adenine using the amidation strategy [68] and further complexed with a uracil substituted ferrocene (figure 17). The presence of corrugations on the nanotube surface was revealed; the complexation

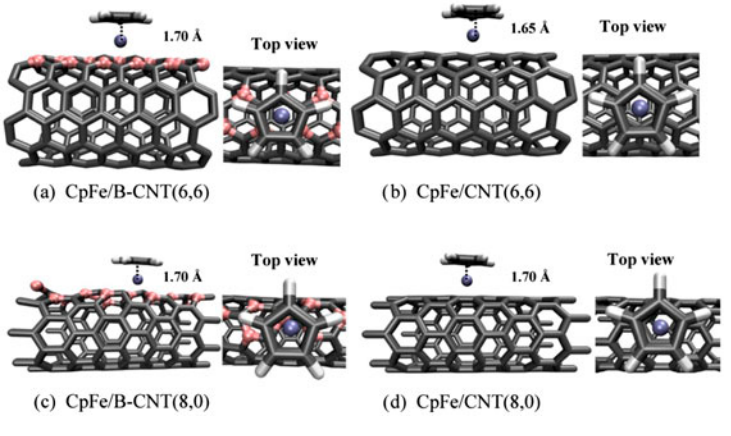

Figure 15. Optimized geometries of CpFe on CNT/B-CNT complexes. Selected distances are shown in units of angstroms, corresponding to the Fe to Cp ring center distance.

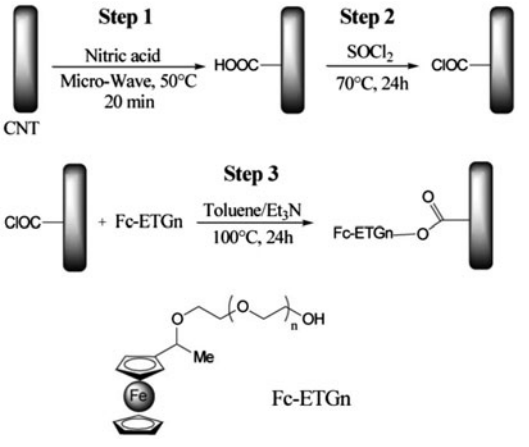

Figure 16. Functionalization process of FWCNT sample by ferrocene derivatives.

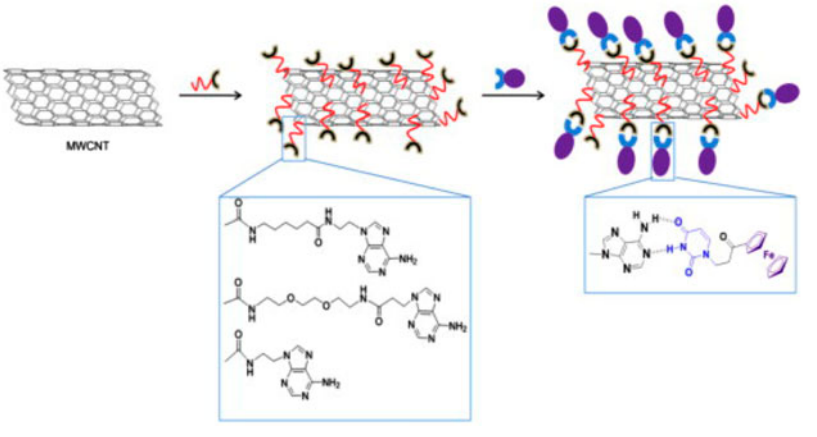

Figure 17. Schematic illustration of the assembly of electroactive ferrocene onto functionalized MWCNTs by exploiting the supramolecular *non-covalent* interactions of adenine–uracil base pairs.

between CNT-bound adenine and uracil was confirmed, as well as the presence of iron from ferrocene on the nanotube surface.

Finally, ferrocene derivatives were *π-stacked* or *covalently grafted* (figure 18) onto a film of CNTs in order to determine the most effective method to immobilize redox centers on those high-surface area electrodes for sensors or catalytic applications [69]. The immobilization of the ferrocene via *π–π* interactions was done with a ferrocene derivative bearing a pyrene **25** group. The covalent grafting on the film of CNTs was achieved in two steps via electroreduction of an aminoethylbenzenediazonium salt followed by post-functionalization with an activated ester derivative of ferrocene. The covalent grafting route gave more redox centers fixed on CNTs than the *π*-stacking

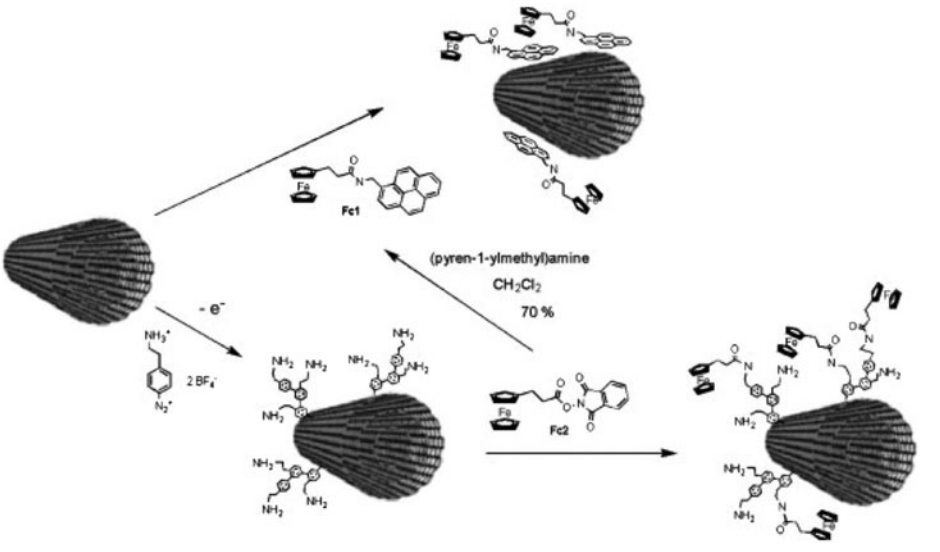

Figure 18. The two methods used to functionalize MWCNTs with ferrocene. Upper – via π–π stacking and lower – via covalent grafting.

one, and the probes were located differently on the electrodes. Comparing both processes, the authors noted that they gave access to immobilized redox molecules on CNTs for a wide variety of applications. The facile π-stacking of pyrene affords attachment of a single monolayer of molecules in a self-assembled manner homogenously divided on the MWCNTs. The covalent derivatization of CNTs with ferrocene moieties unlike the π-stacking one gives a stable and reliable glucose sensor electrode material.

Carbonyls and π-complexes with aromatic compounds

As a classic work in this area, coordinatively unsaturated *Vaska*'s compound **26**, *trans*-chlorocarbonyl-*bis*(triphenylphosphine) iridium(I) [70], was complexed with raw SWCNTs as well as with oxidized, purified nanotubes. The coordination modes were revealed to be different in each case (reaction schemes *12* and *13*). Later on, functionalization of SWCNTs with Vaska's complex containing bromide, *trans*-Ir(CO)Br $(PPh_3)_2$, was investigated by hybrid quantum mechanics/molecular mechanics (QM/MM) calculations [71]. The calculation was not able to find a stable bound adduct between Vaska's complex and the perfect hexagonal network of a (9,0) CNT, thus suggesting that the sidewall is relatively inert to attack from Vaska's complex. However, nanotube end-caps or defective sites on the sidewall show a higher propensity to coordination with the inorganic fragment, indicating such sites as more suitable coordination centers for η^2 bonding, similar to the case of C_{60}. Hence, a stable adduct is more likely to be formed when at least one of the coordinating carbons belongs to a pentagonal ring.

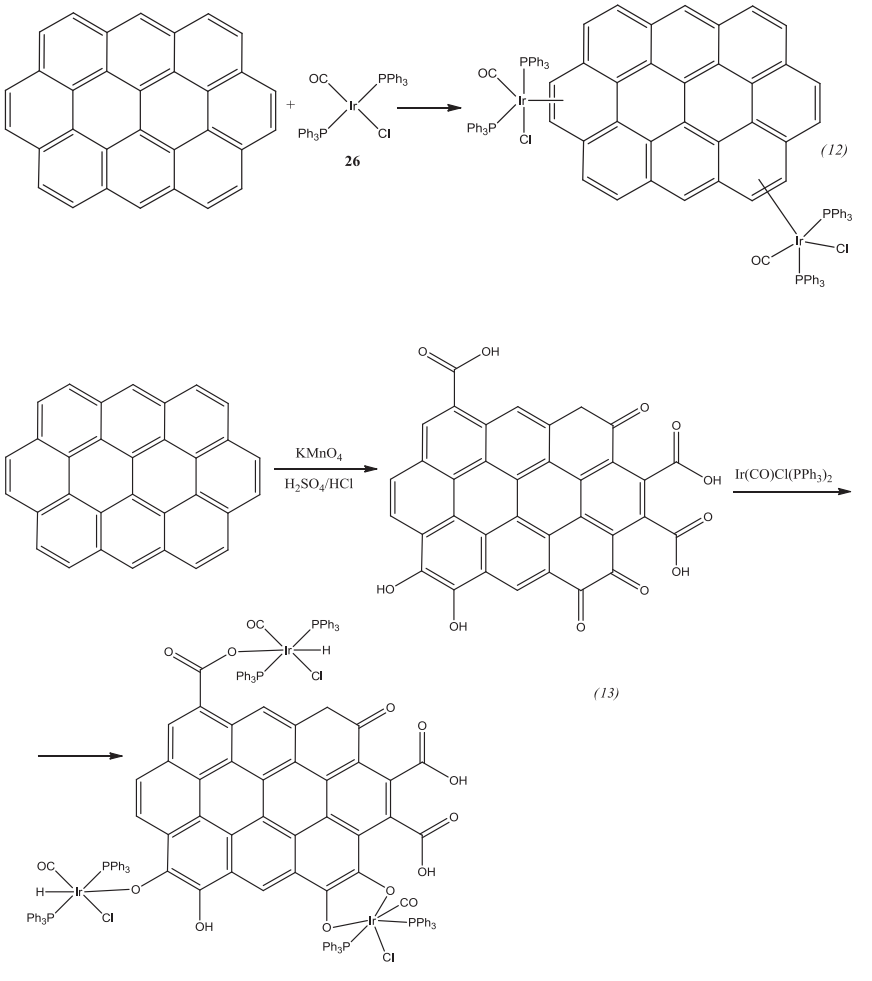

In addition to related chromium complex $[Cp^*Cr(CO)_3]_2$ described in one of the previous sections, organometallic sidewall complexes of pristine and octadecylamine-functionalized SWNTs (reactions *14–17*) were prepared under conditions, which allowed the study of both mono- and *bis*-hexahapto SWNT coordination compounds $[(\eta^6\text{-SWNT})Cr(CO)_3$, $(\eta^6\text{-SWNT})Cr(\eta^6\text{-}C_6H_6)$, $(\eta^6\text{-SWNT})_2Cr]$ (figure 19) [72]. Both endohedral and exohedral modes of chromium complexation to SWCNTs are possible. In the first case, a stable and kinetically inert mode of CNT sidewall bonding with chromium reagents was established, which partially preserves the band electronic structure of the CNTs. The bonding of $Cr(CO)_3$ and $Cr(\eta^6$-benzene) fragments to the SWNTs is primarily covalent in nature, with slight charge transfer character in the case of $Cr(CO)_3$. The electrical conductivity of SWNT thin films was significantly enhanced by sidewall bonding to Group 6 transition metals (M=Cr, Mo, and W), which serve to reduce the inter-CNT junction electrical resistance by formation of SWNT interconnects $[(\eta^6\text{-SWNT})_2\,M]$. Similar results were discussed for related extended periodic π-electron systems: exfoliated graphene (XG), epitaxial graphene, and highly-oriented pyrolytic graphite (HOPG) [73]. In the case of HOPG, $(\eta^6\text{-HOPG})Cr(CO)_3$ was isolated while the XG samples were found to give both $(\eta^6\text{-graphene})_2Cr$ and $(\eta^6\text{-graphene})Cr(CO)_3$.

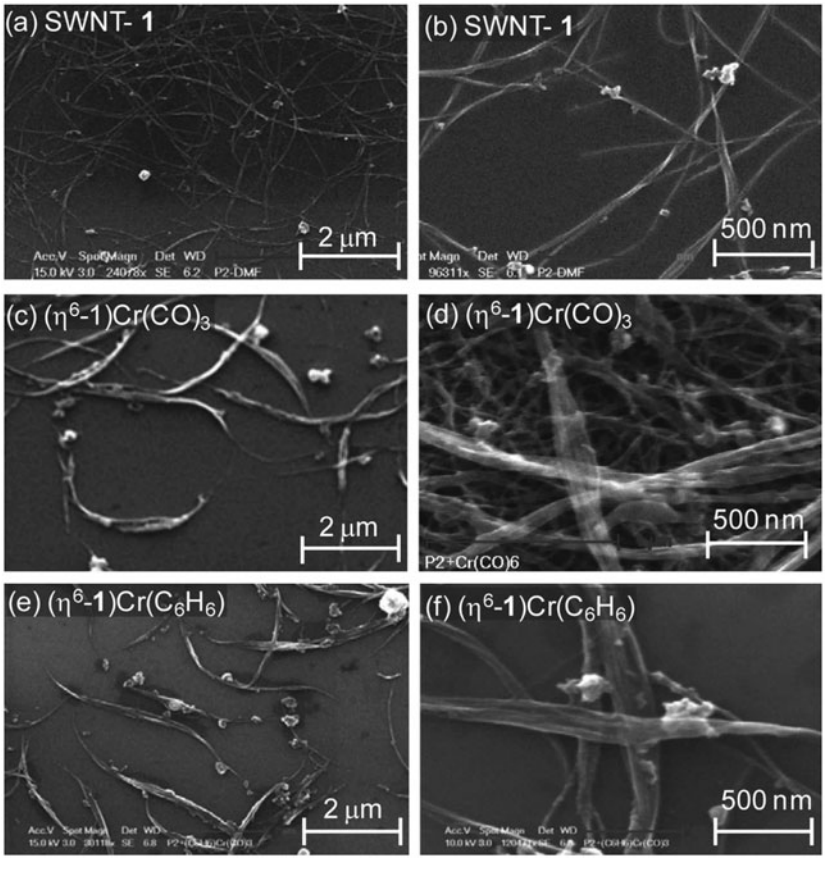

Figure 19. Scanning electron micrographs of: (a–b) pristine SWNTs, (c–d) (η^6-SWNT)-$Cr(CO)_3$, and (e–f) (η^6-SWNT)$Cr(C_6H_6)$.

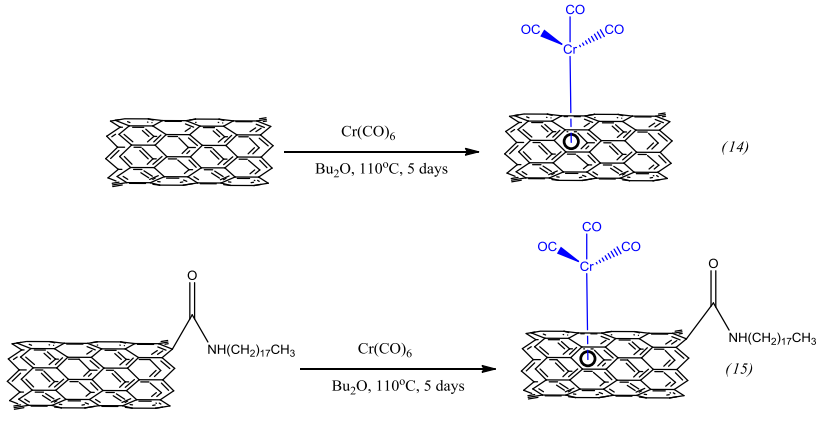

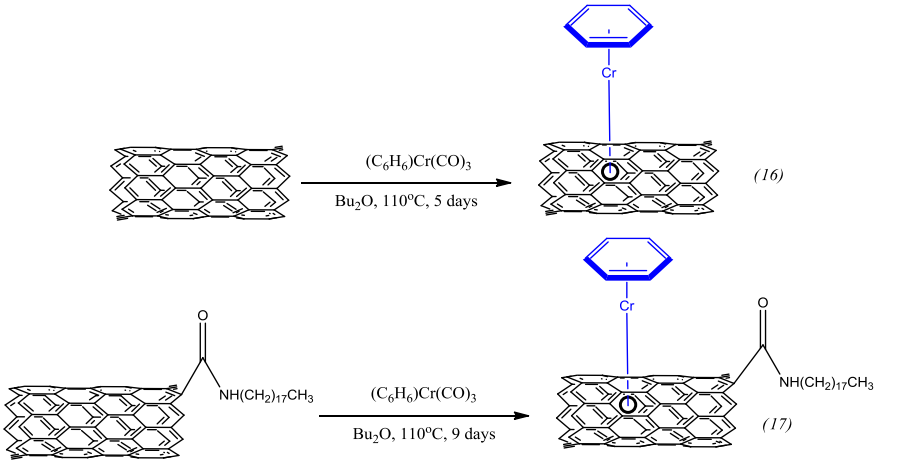

Reactions of SWNT and SWNT-$CONH(CH_2)_{17}CH_3$ with chromium hexacarbonyl and (η^6-benzene)chromium tricarbonyl.

As a theoretical justification for the composites above, first-principles density-functional calculations were employed to study the electronic characteristics of covalently functionalized graphene by metal-*bis*-arene chemistry [74]. Functionalization with M-*bis*-arene (M=Ti, V, Cr, Mn, Fe) molecules led to an opening in the bandgap of graphene (up to 0.81 eV for the Cr derivative), and as a result, transformed it from a semimetal to a semiconductor. The bandgap induced by attachment of a metal topped by a benzene ring was attributed to modification of π-conjugation and depended on the concentration of functionalizing molecules. In a related report [75], the interaction of two organometallic π-aryl (ML_2) complexes, cobaltocene [$Co(\eta^5\text{-}C_5H_5)_2$] and *bis*(benzene) chromium [$Cr(\eta^6\text{-}C_6H_6)_2$], with a series of semiconducting (n,0) ($n = 11$–18) SWNTs was investigated using density-functional theory calculations. Both cobaltocene and *bis*(benzene) chromium act as electron donors to form composites $[ML_2]^{q+}[SWNT]^{q-}$ in which the extent of the charge transfer, and hence the binding energy, is modulated by the diameter and band structure of the nanotube.

All other available literature data correspond to complexes containing a pyrene **25**. In particular, ruthenium polypyridyl complexes, described above, can be modified with pyrene and this way functionalize the CNTs. Thus, the synthesis of a multifunctional block copolymer incorporated with pyrene and ruthenium terpyridyl thiocyanato complex by reversible addition–fragmentation chain transfer polymerization was carried out [76]. The pyrene block in the copolymer facilitates dispersion of MWCNTs in DMF solution because of the strong π–π interaction between the pyrene and nanotube surface (figure 20). The ruthenium complexes greatly enhance the photosensitivity of the functionalized nanotubes in the visible region.

A cobalt-terpyridine transition metal complex, cobalt *bis*(4-pyren-1-yl-*N*-[5-([2,2′;6′,2″] terpyridin-4′-yloxy)-pentyl]-butyramide) **27**, with pendant pyrene moieties was shown to functionalize SWNTs via non-covalent π–π stacking interactions [77]. The non-covalent modification of MWCNTs with pyrene-functionalized nickel complexes **28** through π–π stacking produced robust, noble-metal-free electrocatalytic nanomaterials (figure 21) for H_2

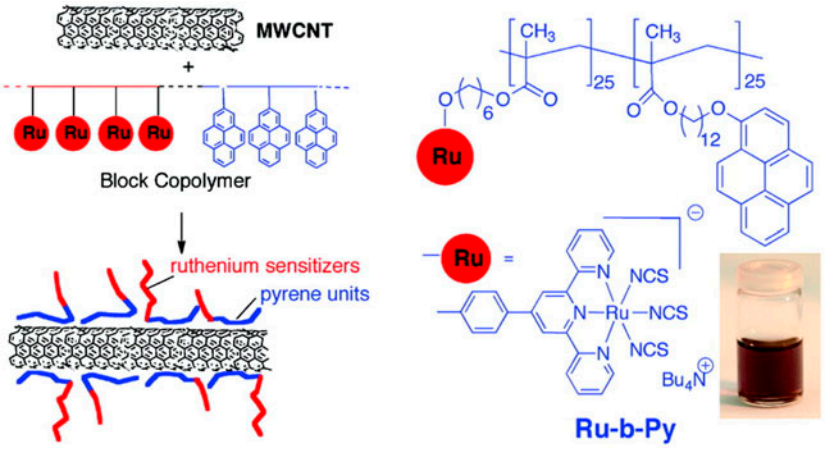

Figure 20. Target block copolymer Ru-b-Py and its functionalization of CNT surface.

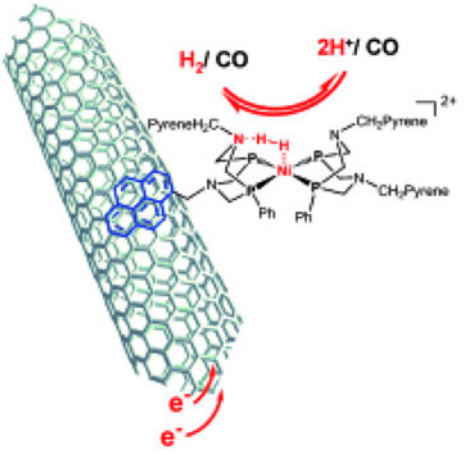

Figure 21. Electrocatalytic nanomaterial on the basis of nickel–pyrene complex.

evolution and uptake [78]. The catalysts were compatible with the conditions encountered in classical proton exchange membrane devices and were tolerant of the common pollutant CO, thus offering significant advantages over traditional Pt-based catalysts. Also, a pyrene-tagged gold(I) complex **29** (reaction scheme *18*) was synthesized and tested as a homogeneous catalyst [79]. Being immobilized onto MWCNTs, this catalyst remained intact on the CNT surface after immobilization and, remarkably, its activity and selectivity in cyclization was not affected in comparison with its homogeneous counterpart. This immobilization through pyrene allowed a "boomerang" effect (figure 22) to take place during catalysis and this effect was found to be strongly dependent on the temperature.

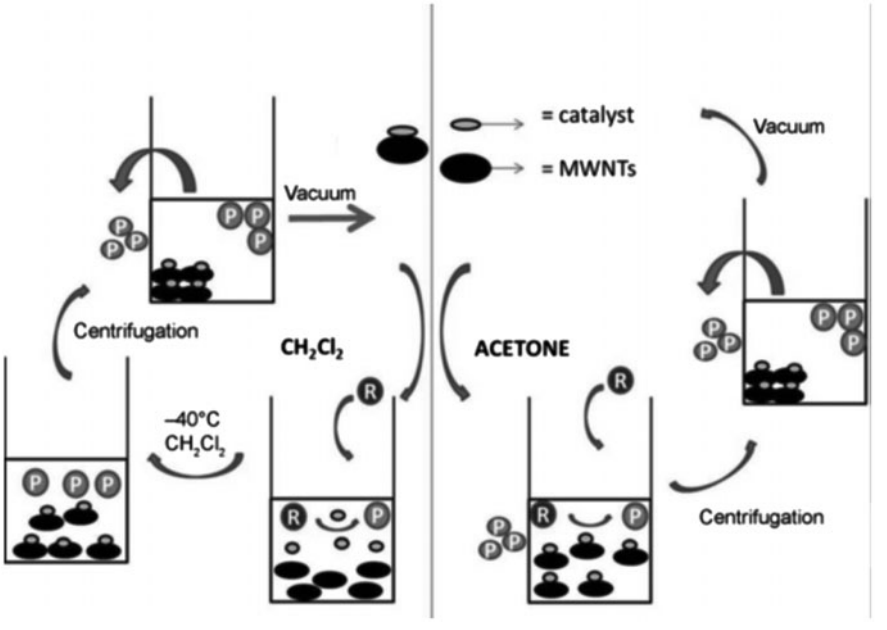

Figure 22. Mechanisms for the boomerang effect (left) and supported homogeneous catalysis (right). R = reagents, P = products.

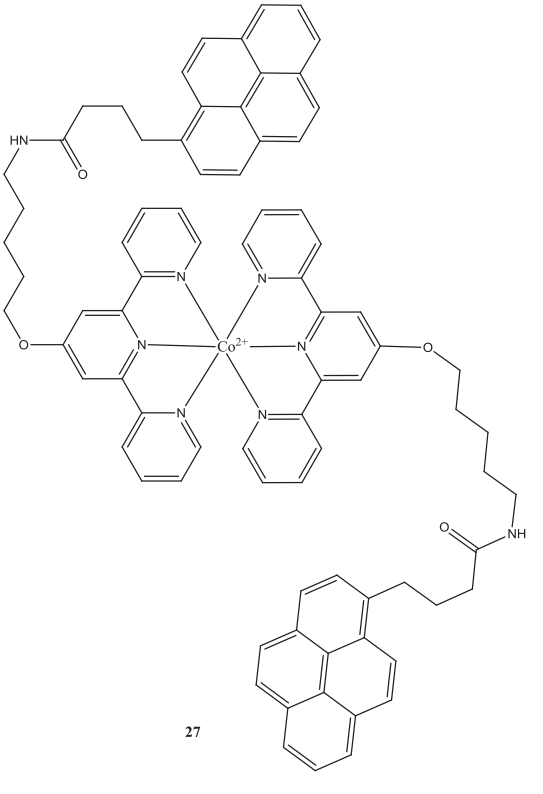

27

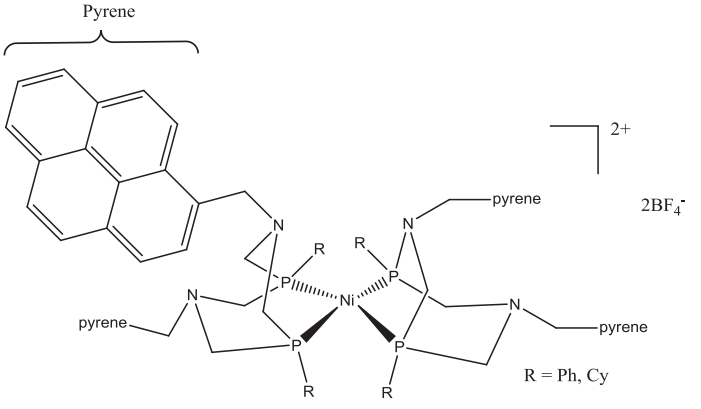

28

Nickel complex containing pyrene moiety

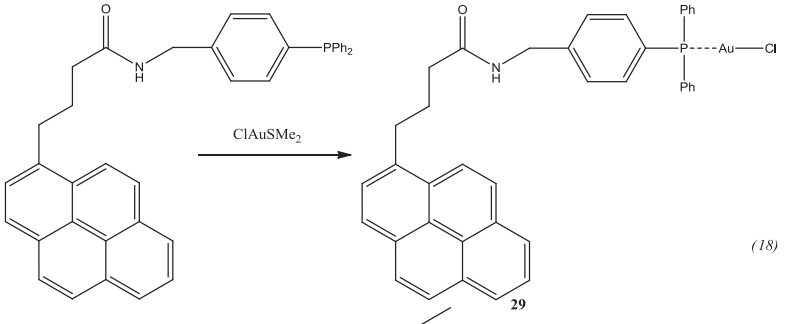

29

Synthesis of the pyrene-tagged gold complex

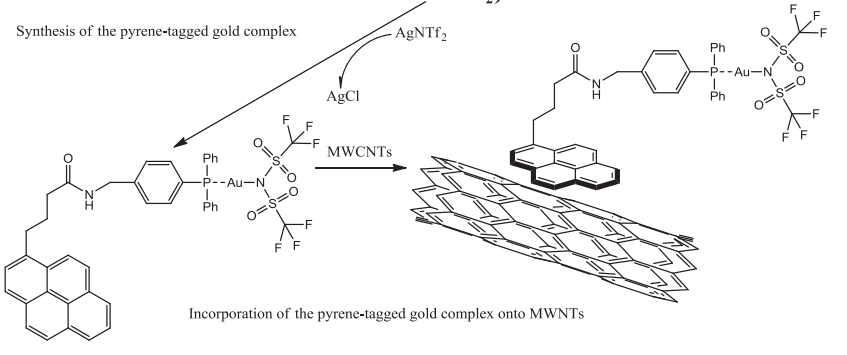

Incorporation of the pyrene-tagged gold complex onto MWNTs

The functionalization of nanostructured graphene-based electrode with [*bis*(2,2′-bipyridine)(4,4′-*bis*(4-pyrenyl-1-ylbutyloxy)-2,2′-bipyridine)]osmium(II) hexafluoro-phosphate complex bearing pyrene groups was carried out [80]. The flexible functionalization of graphene-based electrodes using either supramolecular binding of the Os(II) complex bearing pyrene groups or its electropolymerization via the irreversible oxidation of pyrene was achieved. Thanks to its divalent binding sites, the Os(II) complex constitutes a useful tool to probe the π-extended graphitic surface of RGO (reduced

graphene oxide) and MWCNT films. The Os(II) complex interacts strongly via non-covalent π–π interactions, with π-extended graphene planes **30**, acting as a marker to quantify the electroactive surface of both MWCNT and RGO electrodes and to illustrate their ease of functionalization. Pyrene groups were revealed to be a versatile way of functionalization of nanostructured graphitic carbon electrodes. Similar pyrene-Ru/SWCNT nanohybrid **31** was formed through non-covalent π–π stacking interactions. After oxidative treatment, the pyrene-Ru/SWCNT-functionalized Pt electrode achieved a highly reversible redox process and exhibited excellent electrogenerated chemiluminescence [81]. Due to the high conductivity and high surface area of SWCNTs, the electrogenerated poly-/oligopyrene derivative exhibited enhanced electrochemical behavior with fast electron transfer and highly reversible redox for Ru^{III}/Ru^{II}.

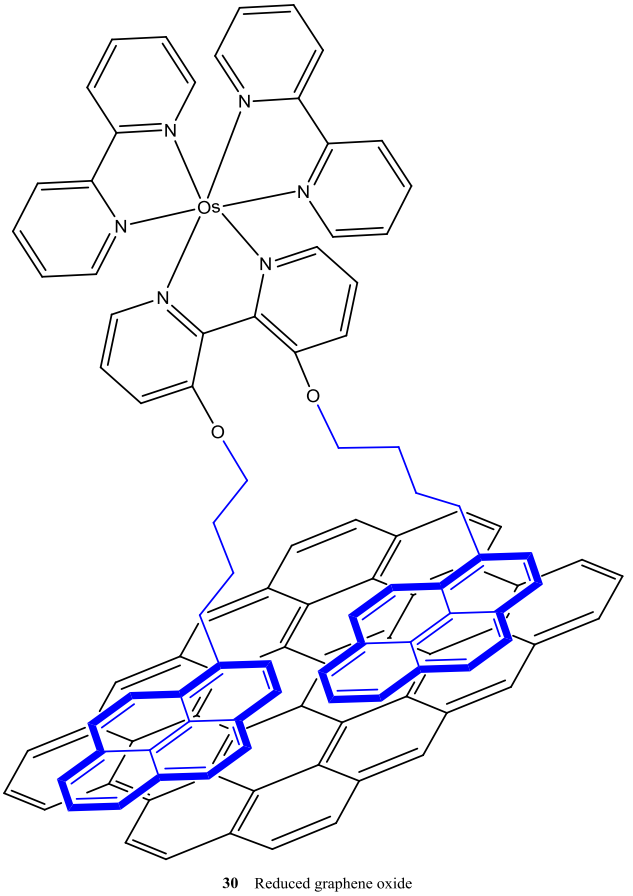

30 Reduced graphene oxide

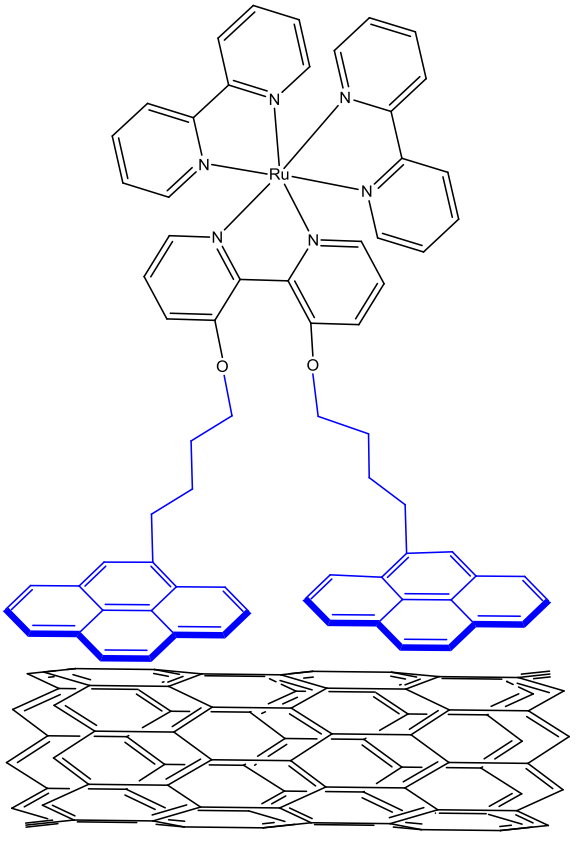

31 Carbon nanotubes

Composites with metal carbene complexes

Oxidized MWCNTs were covalently modified [82] with appropriate hydroxyl-ending imidazolium salts using their carboxylic acid groups and then used to prepare nanohybrid materials containing iridium N-heterocyclic carbene (NHC)-type organometallic complexes **32–33** with efficiencies as high as 95% (reactions *19*). These nanotube-supported iridium–NHC materials were active in the heterogeneous iridium-catalyzed hydrogen-transfer reduction of cyclohexanone to cyclohexanol with 2-propanol/KOH as hydrogen source, being more efficient than related homogeneous catalysts based on acetoxy-functionalized Ir–NHC complexes with initial TOFs up to 5550 h^{-1}. A good recyclability of the catalysts, without loss of activity, and stability in air was observed. The heterogeneous catalysts remained stable through successive catalytic runs.

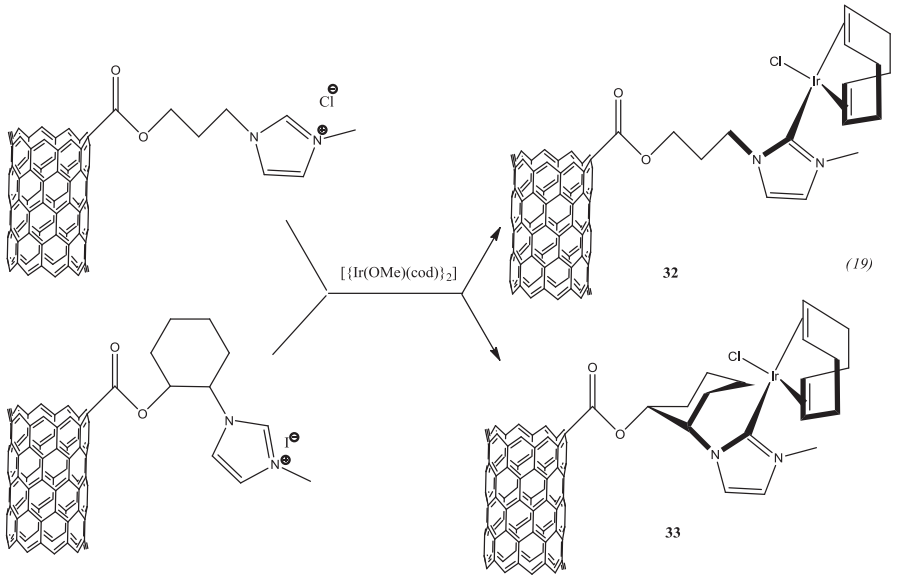

(19)

Synthesis of NHC-iridium complexes anchored on the carbon nanotubes.

Conclusions

CNTs can form hybrids with metal complexes of O-containing ligands (crown ethers and carboxylates), N- and N,O-containing ligands (amines, Schiff bases, polypyridyl compounds, porphyrins, and phthalocyanines), as well as σ- and π-organometallic compounds (carbonyls, cyclopentadienyls, pyrene-containing moieties, and other aromatic structures). The interaction "metal complex – CNTs" could take place via either covalent or non-covalent (π–π-stacking) interactions; in some cases both routes at the same time are possible.

Interesting effects have been discovered for distinct groups of metal complex-CNT composites/hybrids. For example, for polynuclear $\{Mn_4\}$ complexes, the reaction can only be achieved for tubes which were oxidized to create carboxylic groups. The reaction "$\{Mn_4\}$ complex/CNTs" is based on ligand exchange between the ligands of the complex and the carboxylic groups created on the CNTs by oxidation in air. For ferrocene-functionalized CNTs, their mutual interaction could be *covalent, non-covalent, or of both types* at the same time. For a variety of pyrene-containing complexes, their units provide the means for non-covalent functionalization of SWNTs via π–π interactions, ensuring that the electronic properties of SWNTs are not impacted by chemical modification of the carbon skeleton.

DFT calculations also revealed intriguing aspects of "metal complex/CNT" hybrids. For instance, both cobaltocene and *bis*(benzene) chromium act as electron donors to form composites $[ML_2]^{q+}[SWNT]^{q-}$ in which the extent of the charge transfer, and hence the binding energy, is modulated by the diameter and band structure of the nanotube. Another example is an iron porphyrin FeP on different surfaces of SWCNTs. Two mechanisms for the FeP attachment on metallic and semiconducting CNTs were considered; physisorption through π–π-stacking interaction and chemisorption through sp^2 and sp^3 bonding configurations.

In addition to "real" "metal complex/CNT" hybrids, investigations of porphyrin-like defects in CNTs surface have led to conclusions about their strong binding to hydrogen (this can act as a media for storing hydrogen) or an excellent oxygen reduction catalytic activity. A very important aspect is related to the *solubility* (more exactly, *dispersibility*) [83] of formed composites "metal complex/CNTs." Thus, in the case of CNTs/crown ether complexes with alkaline metals, the ionic interaction leads to a considerable increase in the solubility of SWCNTs in both organic and aqueous solvents such as ethanol, DMSO, DMF, and H_2O. Dispersion of SWCNTs was also achieved in the presence of water soluble ruthenium polypyridyl complexes and non-TPP type porphyrins.

We emphasized the rich variety of applications of the discussed CNTs/metal complex hybrids. For example, oxidation of primary and secondary alcohols, and use of non-precious electrocatalysts for the electroreduction of oxygen have high value. Gas and ECL sensors for Pb^{2+} determination, Hg^{2+} retaining, uptake of CO_2 and CH_4, carbon paste electrodes, molecular memory devices, or nanohybrid circuits are also applications.

References

[1] P. Pérez. *Alkane C–H Activation by Single-site Metal Catalysis (Catalysis by Metal Complexes)*, p. 200, Springer, New York (2012).
[2] W. Rehman, N. Bashir. *Transition Metal Complexes: The Future Medicines: Synthetic Route and Bioassay of Transition Metal Complexes*, p. 64, VDM Verlag Dr. Müller (2010).
[3] N. Hadjiliadis, E. Sletten (Eds.). *Metal Complex – DNA Interactions*, p. 544, Wiley-Blackwell, Hoboken, NJ (2009).
[4] A.D. Pomogailo. *Catalysis by Polymer-immobilized Metal Complexes*, p. 424, CRC Press, Boca Raton, FL (1999).
[5] B.M. Andreev. *Separation of Isotopes of Biogenic Elements in Two-phase Systems*, p. 316, Elsevier Science, New York (2007).
[6] H. Bradl. *Heavy Metals in the Environment: Origin, Interaction and Remediation*, Vol. 6 (Interface Science and Technology), Elsevier Science, Amsterdam, p. 282 (2005).
[7] D. Jain, A. Saha, A.A. Martí. *Chem. Commun.*, **47**, 2246 (2011).
[8] X. Peng, H. Qin, L. Li, Y. Huang, J. Peng, Y. Cao, N. Komatsu. *J. Mater. Chem.*, **22**, 5764 (2012).
[9] J. Cheng, X.P. Zou, G. Zhu, M.F. Wang, Y. Su, G.Q. Yang, X.M. Lu. *Solid State Commun.*, **149**, 1619 (2009).
[10] M.C. Schnitzler, M.M. Oliveira, D. Ugarte, A.J.G. Zarbin. *Chem. Phys. Lett.*, **381**, 541 (2003).
[11] V. Georgakilas, D. Gournis, V. Tzitzios, L. Pasquato, D.M. Guldi, M. Prato. *J. Mater. Chem.*, **17**, 2679 (2007).
[12] D. Kocsis, D. Kaptas, A. Botos, A. Pekker, K. Kamaras. *Phys. Status Solidi B*, **248**, 2512 (2011).
[13] C. Backes. *Noncovalent Functionalization of Carbon Nanotubes: Fundamental Aspects of Dispersion and Separation in Water*, p. 260, Springer, New York (2012).
[14] P.J.F. Harris. *Carbon Nanotube Science: Synthesis, Properties and Applications*, 2nd Edn, p. 314, Cambridge University Press, Cambridge (2011).
[15] L. Meng, C. Fu, Q. Lu. *Prog. Nat. Sci.*, **19**, 801 (2009).
[16] S. Banerjee, T. Hemraj-Benny, S.S. Wong. *Adv. Mater.*, **17**, 17 (2005).
[17] R.E. Anderson, A.R. Barron. *J. Nanosci. Nanotechnol.*, **7**, 3646 (2007).
[18] G. Kerric, E.J. Parra, G.A. Crespo, F.X. Riusa, P. Blondeau. *J. Mater. Chem.*, **22**, 16611 (2012).
[19] A. Khazaei, M.K. Borazjani, K.M. Moradian. *J. Chem. Sci.*, **124**, 1127 (2012).
[20] Y. Wang, Y. Wu, J. Xie, H. Gea, X. Hu. *Analyst*, **138**, 5113 (2013).
[21] Z. Xiang, Z. Hu, D. Cao, W. Yang, J. Lu, B. Han, W. Wang. *Angew. Chem. Int. Ed.*, **50**, 491 (2011).
[22] A. Okia, L. Adamsa, Z. Luod, E. Osayamena, P. Bineyb, V. Khabashesku. *J. Phys. Chem. Solids*, **69**, 1194 (2008).
[23] M. Soleimani, M. Ghahraman Afshar, A. Sedghi. *ISRN Nanotechnol.*, Article ID 674289, **2013**, 8 (2013).
[24] S. Hyun Yoon, J. Hoon Han, B. Kun Kim, H. Nim Choi, W.-Y. Lee. *Electroanalysis*, **22**, 1349 (2010).
[25] Y. Tao, Z.-J. Lin, X.-M. Chen, X.-L. Huang, M. Oyama, X. Chen, X.-R. Wang. *Sens. Actuators, B*, **129**, 758 (2008).
[26] D. Jain, A. Sahaac, A.A. Martí. *Chem. Commun.*, **47**, 2246 (2011).
[27] R. Martín, L. Jiménez, M. Alvaro, J.C. Scaiano, H. Garcia. *Chem. – Eur. J.*, **16**, 7282 (2010).
[28] R. Rajarao, T.H. Kim, B. Ramachandra Bhat. *J. Coord. Chem.*, **65**, 2671 (2012).
[29] M. Salavati-Niasari, M. Bazarganipour. *Transition Met. Chem.*, **34**, 605 (2009).
[30] M. Salavati-Niasari, M. Bazarganipour. *Appl. Surf. Sci.*, **255**, 2963 (2008).
[31] M. Salavati-Niasari, M. Bazarganipour. *Bull. Korean Chem. Soc.*, **30**, 355 (2009).
[32] G. Magadur, J.-S. Lauret, G. Charron, F. Bouanis, E. Norman, V. Huc, C.-S. Cojocaru, S. Gomez-Coca, E. Ruiz, T. Mallah. *J. Am. Chem. Soc.*, **134**, 7896 (2012).

[33] M. Navidi, B. Movassagh, S. Rayati. *16th International Electronic Conference on Synthetic Organic Chemistry*, Basel, 1–30 November (2012).
[34] H.-J. Lee, W.S. Choi, T. Nguyen, Y.B. Lee, H. Lee. *Carbon*, **49**, 5150 (2011).
[35] H. Liu, Y. Cui, P. Li, Y. Zhou, X. Zhu, Y. Tang, Y. Chen, T. Lu. *Analyst*, **138**, 2647 (2013).
[36] C. Meyer, C. Besson, R. Frielinghaus, A.-K. Saelhoff, H. Flototto, L. Houben, P. Kogerler, C.M. Schneider. *Phys. Status Solidi B*, **249**, 2412 (2012).
[37] X.M. Tu, S.L. Luo, X.B. Luo, Y.J. Zhao, L. Feng, J.H. Li. *Sci. China Chem.*, **54**, 1319 (2011).
[38] C. Yang, Y. Chai, R. Yuan, J. Guo, F. Jia. *Anal. Sci.*, **28**, 275 (2012).
[39] E.M.N. Mhuircheartaigh, S. Giordani, D. MacKernan, S.M. King, D. Rickard, L.M. Val Verde, M.O. Senge, W.J. Blau. *J. Nanotechnol.*, Article ID 745202, **2011**, 12 (2011). doi:10.1155/2011/745202
[40] Y. Kim, S.O. Kim, W. Lee, D. Lee, W. Lee. US Patent 20130030175 (2013).
[41] O. Ito, F. D'Souza. *Molecules*, **17**, 5816 (2012).
[42] L. Lvova, M. Mastroianni, G. Pomarico, M. Santonico, G. Pennazza, C. Di Natale, R. Paolesse, A. D'Amico. *Sens. Actuators, B*, **170**, 163 (2012).
[43] D.M. Guldi, G.M. Aminur Rahman, S. Qin, M. Tchoul, W.T. Ford, M. Marcaccio, D. Paolucci, F. Paolucci, S. Campidelli, M. Prato. *Chem. Eur. J.*, **12**, 2152 (2006).
[44] X. Peng, H. Qin, L. Li, Y. Huang, J. Peng, Y. Cao, N. Komatsu. *J. Mater. Chem.*, **22**, 5764 (2012).
[45] I. Ruiz-Tagle, W. Orellana. *Phys. Rev. B*, **82**, 115406 (2010).
[46] J. Yu, S. Mathew, B.S. Flavel, J.S. Quinton, M.R. Johnston, J.G. Shapter, *International Conference on Nanoscience and Nanotechnology*, Melbourne, ICONN 2008, pp. 176–179 (2008).
[47] D.-M. Ren, Z. Guo, F. Du, Z.-F. Liu, Z.-C. Zhou, X.-Y. Shi, Y.-S. Chen, J.-Y. Zheng. *Int. J. Mol. Sci.*, **9**, 45 (2008).
[48] M. Mananghaya. *Int. J. Sci. Eng. Res.*, **4**, 4 (2013).
[49] D. Hyun Lee, W. Jun Lee, W. Jong Lee, S. Ouk Kim, Y.-H. Kim. *Phys. Rev. Lett.*, Article ID 175502, **106**, 4 (2011).
[50] A.Yu. Tolbin, V.N. Khabashesku, L.G. Tomilova. *Mendeleev Commun.*, **22**, 59 (2012).
[51] I. Kruusenberg, L. Matisen, K. Tammeveski. *Int. J. Electrochem. Sci.*, **8**, 1057 (2013).
[52] I. Kruusenberg, L. Matisen, K. Tammeveski. *J. Nanosci. Nanotechnol.*, **13**, 621 (2013).
[53] W. Orellana. *Chem. Phys. Lett.*, **541**, 81 (2012).
[54] Y. Yuan, B. Zhao, Y. Jeon, S. Zhong, S. Zhou, S. Kim. *Bioresour. Technol.*, **102**, 5849 (2011).
[55] G. Dong, M. Huang, L. Guan. *Phys. Chem. Phys.*, **14**, 2557 (2012).
[56] Y. Wang, N. Hu, Z. Zhou, D. Xu, Z. Wang, Z. Yang, H. Wei, E. Siu-Wai Kong, Y. Zhang. *J. Mater. Chem.*, **21**, 3779 (2011).
[57] L. Zhang, H. Yu, L. Liu, L. Wang. *J. Composite Mater.*, (in press).
[58] J. Bartelmess, B. Ballesteros, G. de la Torre, D. Kiessling, S. Campidelli, M. Prato, T. Torres, D.M. Guldi. *J. Am. Chem. Soc.*, **132**, 16202 (2010).
[59] R.O. Ogbodu, E. Antunesa, T. Nyokong. *Dalton Trans.*, **42**, 10769 (2013).
[60] K. Malika Tripathi, A. Begum, S. Kumar Sonkar, S. Sarkar. *New J. Chem.*, **37**, 2708 (2013).
[61] S. Park, S. Woong Yoon, K.-B. Lee, D. Jin Kim, Y. Hwan Jung, Y. Do, H.-J. Paik, I.S. Choi. *Macromol. Rapid Commun.*, **27**, 47 (2006).
[62] D. Priftis, N. Petzetakis, G. Sakellariou, M. Pitsikalis, D. Baskaran, J.W. Mays, N. Hadjichristidis. *Macromolecules*, **42**, 3340 (2009).
[63] A.S. Lobach, R.G. Gasanov, E.D. Obraztsova, A.N. Shchegolikhin, V.I. Sokolov. *Fullerenes, Nanotubes, Carbon Nanostruct.*, **13**, 287 (2005).
[64] Z. Zhang, C. Heath Turner. *J. Phys. Chem. C*, **117**, 8758 (2013).
[65] A. Chernov, M. Havlicek, W. Jantsch, M.H. Rümmeli, A. Bachmatiuk, K. Yanagi, H. Peterlik, H. Kataura, F. Sauerzopf, R. Resel, F. Simon, H. Kuzmany. *Phys. Status Solidi B*, **249**, 2323 (2012).
[66] X.-J. Huang, H.-S. Im, D.-H. Lee, H.-S. Kim, Y.-K. Choi. *J. Phys. Chem. C*, **111**, 1200 (2007).
[67] N. Allali, V. Urbanova, V. Mamane, J. Waldbock, M. Etienne, M. Mallet, X. Devaux, B. Vigolo, Y. Fort, A. Walcarius, M. Noel, A.V. Soldatov, E. McRae, M. Dossot. *Phys. Status Solidi B*, **249**, 2349 (2012).
[68] P. Singh, C. Menard-Moyon, J. Kumar, B. Fabre, S. Verma, A. Bianco. *Carbon*, **50**, 3170 (2012).
[69] A. Le Goff, F. Moggia, N. Debou, P. Jegou, V. Artero, M. Fontecave, B. Jousselme, S. Palacin. *J. Electroanal. Chem.*, **641**, 57 (2010).
[70] S. Banerjee, S.S. Wong. *Nano Lett.*, **2**, 49 (2002).
[71] F. Mercuri, A. Sgamellotti. *J. Phys. Chem. B*, **110**, 15291 (2006).
[72] I. Kalinina, E. Bekyarova, S. Sarkar, F. Wang, M.E. Itkis, X. Tian, S. Niyogi, N. Jha, R.C. Haddon. *Macromol. Chem. Phys.*, **213**, 1001 (2012).
[73] S. Sarkar, S. Niyogi, E. Bekyarova, R.C. Haddon. *Chem. Sci.*, **2**, 1326 (2011).
[74] P. Plachinda, D.R. Evans, R. Solanki. *J. Chem. Phys.*, Article ID 044103, **135**, 9 (2011).
[75] E.L. Sceats, J.C. Green. *Phys. Rev. B*, Article ID 245441, **75** (2007).
[76] C.H. Li, A.M.C. Ng, C.S.K. Mak, A.B. Djurišić, W.K. Chan. *ACS Appl. Mater. Interfaces*, **4**, 74 (2012).
[77] E.W. McQueen, J.I. Goldsmith. *J. Am. Chem. Soc.*, **131**, 17554 (2009).
[78] P.D. Tran, A. Le Goff, J. Heidkamp, B. Jousselme, N. Guillet, S. Palacin, H. Dau, M. Fontecave, V. Artero. *Angew. Chem., Int. Ed. Engl.*, **50**, 1371 (2011).

[79] C. Vriamont, M. Devillers, O. Riant, S. Hermans. *Chem. – Eur. J.*, **19**, 12009 (2013).
[80] A. Le Goff, B. Reuillard, S. Cosnier. *Langmuir*, **29**, 8736 (2013).
[81] S.-N. Ding, D. Shan, S. Cosnier, A. Le Goff. *Chem. – Eur. J.*, **18**, 11564 (2012).
[82] M. Blanco, P. Álvarez, C. Blanco, M.V. Jiménez, J. Fernández-Tornos, J.J. Pérez-Torrente, L.A. Oro, R. Menéndez. *ACS Catal.*, **3**, 1307 (2013).
[83] O.V. Kharissova, B.I. Kharisov, E.G. de Casas Ortiz. *RSC Advances*, **3**, 24812 (2013).